

DAMPED LYMAN ALPHA SYSTEMS AT $Z < 1.65$: THE EXPANDED SDSS HST SAMPLE¹

SANDHYA M. RAO^{2,4}, DAVID A. TURNSHEK², AND DANIEL B. NESTOR^{2,3}

Draft version August 3, 2021

ABSTRACT

We present results of our *Hubble Space Telescope* Cycle 11 Survey for low-redshift ($z < 1.65$) damped Ly α systems (DLAs) in the UV spectra of quasars selected from the Sloan Digital Sky Survey Early Data Release. These quasars have strong intervening MgII-FeII systems which are known signatures of high column density neutral gas. In total, including our previous surveys, UV observations of Ly α absorption in 197 MgII systems with $z < 1.65$ and rest equivalent width (REW) $W_0^{\lambda 2796} \geq 0.3$ Å have now been obtained. The main results are: (1) The success rate of identifying DLAs in a MgII sample with $W_0^{\lambda 2796} \geq 0.5$ Å and FeII $W_0^{\lambda 2600} \geq 0.5$ Å is $36(\pm 6)\%$, and increases to $42(\pm 7)\%$ for systems with $W_0^{\lambda 2796}/W_0^{\lambda 2600} < 2$ and MgI $W_0^{\lambda 2852} > 0.1$ Å. (2) The mean HI column density of MgII systems with $0.3 \text{ \AA} \leq W_0^{\lambda 2796} < 0.6 \text{ \AA}$ is $\langle N(\text{HI}) \rangle = (9.7 \pm 2.2) \times 10^{18} \text{ cm}^{-2}$. For the larger REW systems in our sample, $\langle N(\text{HI}) \rangle = (3.5 \pm 0.7) \times 10^{20} \text{ cm}^{-2}$. The mean HI column density remains constant with increasing REW for $W_0^{\lambda 2796} \geq 0.6$ Å, but the fraction of MgII systems containing DLAs is found to increase with increasing REW. (3) By combining our low-redshift results with results at higher redshift from Prochaska and Herbert-Fort and at $z = 0$ from Ryan-Weber et al. we find that we can parameterize the DLA incidence per unit redshift as $n_{\text{DLA}}(z) = n_0(1+z)^\gamma$, where $n_0 = 0.044 \pm 0.005$ and $\gamma = 1.27 \pm 0.11$. This parameterization is consistent with no evolution for $z \lesssim 2$ ($\Omega_\Lambda = 0.7$, $\Omega_M = 0.3$), but exhibits significant evolution for $z \gtrsim 2$. (4) The cosmological neutral gas mass density due to DLAs is constant in the redshift interval $0.5 < z < 5.0$ to within the uncertainties, $\Omega_{\text{DLA}} \approx 1 \times 10^{-3}$. This is larger than $\Omega_{\text{gas}}(z=0)$ by a factor of ≈ 2 . (5) The slope of the HI column density distribution does not change significantly with redshift. However, the low redshift distribution is marginally flatter due to the higher fraction of high column density systems in our sample. (6) Finally, using the precision of MgII survey statistics, we show that under the assumption of constant DLA fraction and HI column density suggested by our current sample, there may be evidence of a decreasing Ω_{DLA} from $z = 0.5$ to $z = 0$. We discuss selection effects that might affect the results from our survey. We reiterate the conclusion of Hopkins, Rao, & Turnshek that very high columns of neutral gas might be missed by DLA surveys because of their very small cross sections, and therefore, that Ω_{DLA} might not include the bulk of the neutral gas mass in the Universe.

Subject headings: galaxies: evolution — galaxies: galaxy formation — quasars: absorption lines

1. INTRODUCTION

Recently, Fukugita & Peebles (2004) have summarized current measurements of the local mass-energy inventory. Of the local baryonic matter, about 6% is stars or their end states, about 4% is hot intracluster x-ray emitting gas, and somewhat less than 2% is neutral or molecular gas. The remainder of the baryonic matter is assumed to be in the form of a warm-hot intergalactic medium (WHIM), with properties similar to those discussed by Cen & Ostriker (1999). However, importantly, processes in the neutral and molecular gas components most directly influence the formation of stars in galaxies. Thus, the determination of empirical results on the distribution and cosmic evolution of neutral hydrogen gas is a key step in better understanding galaxy formation. At present, there are two observational methods to study neutral hydrogen. Locally, the information is ob-

tained through radio observations of HI 21 cm emission. But at large distances (redshift $z > 0.2$) radio sensitivity limitations require that the information be obtained through observations of Ly α absorption in the spectra of background quasars. Intervening damped Ly α (DLA) absorption-line systems in quasar spectra provide important non-local probes of the neutral gas content of the universe since they can, in principle, be tracked from the present epoch all the way back to the farthest detectable quasars. Since the first survey for DLAs nearly two decades ago (Wolfe, Turnshek, Smith, & Cohen 1986), it has been accepted that they contain the bulk of the neutral gas content of the universe. This first survey defined a DLA absorption-line system as an intervening gaseous HI region with neutral hydrogen column density $N(\text{HI}) \geq 2 \times 10^{20} \text{ cm}^{-2}$. The damping wings of the Voigt profile become prominent at column densities near 10^{19} cm^{-2} . Thus, even low-resolution spectra which are useful for the detection of Ly α absorption lines with rest equivalent widths (REWs) ≥ 10 Å can be adopted to perform DLA searches, and subsequent studies have used this threshold to describe the statistics of DLAs (Lanzetta et al. 1991; Rao & Briggs 1993; Lanzetta, Wolfe, & Turnshek 1995; Rao, Turnshek, & Briggs 1995, henceforth RTB95; Rao & Turnshek 2000, henceforth RT00; Storrie-

¹ Based on data obtained from the Sloan Digital Sky Survey (SDSS) and on observations made with the Hubble Space Telescope (HST) operated by STScI-AURA for NASA.

² Department of Physics & Astronomy, University of Pittsburgh, Pittsburgh, PA 15260

³ Astronomy Department, University of Florida, Gainesville, FL 32611

⁴ email: rao@everest.phyast.pitt.edu

Lombardi & Wolfe 2000; Péroux et al. 2003; Prochaska & Herbert-Fort 2004). The $N(HI) \gtrsim 10^{20} \text{ cm}^{-2}$ limit is believed to be the threshold above which the gas becomes predominantly neutral and conducive for future star formation.

The conclusion that DLA surveys identify the bulk of the neutral gas in the universe is based on three results or assumptions. First, integration of the DLA HI column density distribution shows that a relatively small fraction of the neutral gas is contributed by Lyman limit and sub-DLA absorption systems with $3 \times 10^{17} < N(HI) < 2 \times 10^{20} \text{ cm}^{-2}$, at least for $z < 3.5$ (Péroux et al. 2003, 2005), and perhaps at all redshifts (Prochaska & Herbert-Fort 2004). Second, dust obscuration does not cause DLA surveys to miss a large fraction of the neutral gas (Ellison et al. 2001, 2004). Third, the biases introduced by gas cross section selection are small. However, with regard to this last point, it is important to emphasize that the interception (or discovery) probability is the product of gas cross section times comoving absorber number density, and no DLAs with $N(HI) > 8 \times 10^{21} \text{ cm}^{-2}$ have been discovered. Thus, the third assumption requires that rare systems with relatively low gas cross section and very high HI column density are either absent or have not been missed to the extent that the neutral gas mass density will be significantly underestimated by quasar absorption line surveys. But this assumption might have to be reevaluated in order to explain the discrepancy between the star formation history (SFH) of DLAs as inferred from their HI column densities and that determined from galaxies that trace the optical luminosity function (Hopkins, Rao, & Turnshek 2005). We will, therefore, address the validity of this assumption later.

Our main purpose in this paper is to present the results of the most extensive survey for low-redshift DLAs to date. Since the Ly α line falls in the UV for redshifts $z < 1.65$, Hubble Space Telescope (HST) spectroscopy is needed to detect and measure DLAs in this redshift regime that corresponds to the last $\approx 70\%$ of the age of the universe. Coupled with the fact that DLAs are rare, the scarcity of available HST time has meant that a good statistical description of the neutral gas content at low redshift is lacking. Now, with the Space Telescope Imaging Spectrograph (STIS) out of commission and the installation of the Cosmic Origins Spectrograph (COS) on HST only a remote possibility, further progress with UV spectroscopy seems unlikely, at least for the foreseeable future.

To implement a low-redshift DLA survey with HST we have used an approach which differs from the conventional blind searches for quasar absorption lines. RTB95 developed a method to determine the statistical properties of low-redshift DLAs by bootstrapping from known MgII absorption-line statistics. A similar approach was originally used by Briggs & Wolfe (1983) in an attempt to find 21 cm absorbers towards radio-loud quasars. It has been appreciated for some time that strong MgII-FeII systems generally have HI column densities in excess of 10^{19} cm^{-2} (e.g., Bergeron & Stasińska 1986). Thus, since all high-redshift DLAs are known to be accompanied by low-ionization metal-line absorption (e.g., Turnshek et al. 1989, Lu et al. 1993, Wolfe et al. 1993, Lu & Wolfe 1994, Prochaska et al. 2003a and references

therein), a UV spectroscopic survey for DLAs can be accomplished efficiently if the search is restricted to quasars whose spectra have intervening low-ionization metal-line absorption. Since the MgII $\lambda\lambda 2796, 2803$ absorption doublet can be studied optically for redshifts $z > 0.11$, MgII turns out to be an ideal tracer for low-redshift DLAs. If the incidence of metal lines is known, then the fraction of DLAs in the metal-line sample gives the incidence of DLAs. We further developed this method in RT00, and accomplished a three-fold increase in the number of low-redshift DLAs. We can now confidently use metal absorption-line properties as a predictor for the presence of DLAs.

In this paper we present results from a sample of nearly 200 MgII systems with UV spectroscopy. Most of these data were obtained by us during the course of HST Guest Observer programs to make low-redshift surveys for DLAs. In principle, once DLAs are identified, follow-up observations can reveal details of a DLA's element abundances, kinematic environment, associated galaxy (i.e., a so-called DLA galaxy), star formation rate, temperature, density, ionization state, and size. For example, there is now clear evidence that the neutral gas phase element abundances are increasing from high to low redshift (e.g., Prochaska et al. 2003b, Rao et al. 2005). There is a clear trend which indicates that DLAs residing in regions exhibiting larger kinematic spread have higher element abundances (Nestor et al. 2003; Turnshek et al. 2005). At low redshift ($z < 1$), it is now usually possible to identify the DLA galaxy through imaging (e.g., Rao et al. 2003). At high redshift, high spectral resolution observations can be used to test dynamical models for DLA galaxies (Prochaska & Wolfe 1998). When the background quasar is radio loud, observations of 21 cm absorption provide important results on gas temperature (e.g., Kanekar & Chengalur 2003). Observational constraints on physical conditions (temperature, density, ionization) also come from high-resolution spectroscopy, and this has led to estimates of star formation rates in individual objects (Wolfe, Prochaska, & Gawiser 2003). Estimates on the contribution of DLAs to the cosmic SFH have also been made (Hopkins, Rao, & Turnshek 2005). Finally, observations along multiple closely-spaced sightlines have led to estimates of DLA region sizes (Monier, Turnshek, & Rao 2005). Through such follow-up work, our knowledge of the characteristic properties of the neutral gas component is steadily improving.

Thus, our results serve two purposes. First, they provide a comprehensive up-to-date list of more than 40 low-redshift ($z < 1.65$) DLAs suitable for follow-up studies. Second, they provide information on the distribution and cosmic evolution of neutral gas corresponding to the last $\approx 70\%$ of the age of the universe. We discuss the MgII sample in §2. The DLA sample is presented in §3, followed by statistical results derived from these systems in §4. Notably our study finds no evidence for evolution of the neutral gas mass of the universe between $0.5 < z < 5$; at $z = 0$ the neutral gas mass is now estimated to be a factor of ≈ 2 lower. Moreover, at $z \lesssim 2$ there is no evidence for evolution in the product of absorber comoving number density and gas cross section, but at $z \gtrsim 2$ there is clear evidence for an increase in this quantity in comparison to no evolution models. A discussion of these and other new results is presented in §5. Conclusions are

summarized in §6.

2. THE MGII SAMPLE

The sample of MgII lines used in our earlier DLA surveys (RTB95; RT00) was culled from the literature. We observed 36 quasars that have 60 intervening MgII absorption systems with MgII $\lambda 2796$ REWs $W_0^{\lambda 2796} \geq 0.3$ Å using HST-FOS in Cycle 6 (PID 6577). Twenty one of these MgII systems fell in spectral regions with no flux because of intervening Lyman limit systems. Of the remaining 39 systems, 9 were DLAs. With the addition of UV archival data, the total sample of MgII systems with UV Ly α information included 82⁵ systems of which 12 were DLAs. We found that all DLAs in this survey, with the exception of one, had MgII $W_0^{\lambda 2796}$ and FeII $W_0^{\lambda 2600}$ greater than 0.5 Å. Based on this result, we conducted a similar survey of 54 MgII systems in 37 quasars with HST-STIS in Cycle 9 (PID 8569). Most of these satisfied the strong MgII-FeII criterion for DLAs. Twenty seven had useful UV spectra and four of these were DLAs. The DLA towards Q1629+120 was discovered in this survey and was reported in Rao et al. (2003). Results on the other systems from Cycle 9 are included in this paper.

Further progress could only be made if the sample size was increased several fold. The Sloan Digital Sky Survey (SDSS) sample of quasars, which numbered in the thousands when this phase of our MgII-DLA project began, presented an unprecedented leap in the number of available survey quasars. The previous largest MgII survey by Steidel & Sargent (1992; SS92) used a sample of 103 quasars. The SDSS Early Data Release included nearly 4000 quasars. Nestor (2004) used SDSS-EDR quasar spectra to search for MgII systems with the aim of quantifying the statistical properties of a large MgII sample (Nestor, Turnshek, & Rao 2005, henceforth NTR05) and to conduct follow-up work to search for DLAs. In Cycle 11 (PID 9382), we targeted a sample of 83 MgII systems with $W_0^{\lambda 2796} \geq 1$ Å in 75 SDSS quasars with SDSS magnitude $g \lesssim 19$. There were an additional 16 weaker MgII systems observable in the same set of spectra. Overall, useful UV information was obtained for 88 systems, 25 of which are DLAs. Given the large sample from which quasars could be selected for observation, we were able to minimize the occurrence of intervening Lyman limit absorption by restricting $z_{em} - z_{abs}$ to be small. Nevertheless, we were unable to observe the Ly α line for 11 MgII systems either due to Lyman limits, an intrinsic broad absorption line trough at the position of Ly α absorption in one case, or due to the demise of STIS. Table 1 gives the details of the MgII systems that have UV spectroscopic information. Our entire sample of 197 MgII systems is included. Details of the quasar are given in columns 1, 2, and 3. Columns 4-8 give the absorption

⁵ Of the 87 systems reported in Table 4 of RT00, four systems have been eliminated for reasons noted below, and one was reobserved in HST-Cycle 9. The $z_{abs} = 0.1602$ system towards 0151+045 is a biased system because the galaxy-quasar pair was known prior to the identification of the MgII system. The $z_{abs} = 0.213$ system towards 1148+386 and the 0.1634 system towards 1704+608 were flagged as doubtful systems by Boissé et al. (1992). Also, on closer inspection, the IUE archival spectrum of 1331+170 was inconclusive with regard to the Ly α line of the $z_{abs} = 1.3284$ system. Therefore, these four were eliminated from our current MgII sample. The $z_{abs} = 1.1725$ system towards 1421+330 is the one that was reobserved in Cycle 9.

line information obtained either from the literature (column 9 gives the reference) or from SDSS quasar spectral analysis (NTR05). Column 10 is the $N(HI)$ measurement from the UV spectrum, column 11 is the selection criterion flag used to determine DLA statistics, and column 12 gives the source of the UV spectrum.

We now explain the selection criteria used to include MgII systems in our sample. The total sample is divided into 4 sub-samples which essentially arose from the process of redefining and improving upon our selection process. Our first surveys, described in RTB95 and RT00, included strong MgII systems from the literature; the threshold REWs were chosen to match the MgII sample of SS92 so that their statistical results could be used to determine the incidence of DLA systems. As demonstrated in RT00, if the incidence of MgII systems is known, then the fraction of DLAs in a MgII sample gives the incidence of DLAs. We found that half of the MgII systems in our sample with $W_0^{\lambda 2796} > 0.5$ Å and $W_0^{\lambda 2600} > 0.5$ Å were DLAs, and thus, modified our selection criteria to include a threshold FeII $\lambda 2600$ REW criterion as well. However, we retained the MgII REW thresholds at 0.3 Å, 0.6 Å, and 1.0 Å.

The sub-samples are defined by the following criteria:

1. $W_0^{\lambda 2796} \geq 0.3$ Å;
2. $W_0^{\lambda 2796} \geq 0.6$ Å;
3. $W_0^{\lambda 2796} \geq 0.6$ Å and $W_0^{\lambda 2600} \geq 0.5$ Å; and
4. $W_0^{\lambda 2796} \geq 1.0$ Å and $W_0^{\lambda 2600} \geq 0.5$ Å.

Sub-sample 1 includes all systems surveyed in RT00, as well as additional systems that happened to fall along quasar sightlines that were targeted due to the presence of another stronger system from sub-samples 2, 3, or 4. Sub-samples 2 and 3 were mainly targeted for observation in HST-Cycle 9, and sub-sample 4 includes systems found in SDSS-EDR spectra and observed in HST-Cycle 11. A few systems from the SDSS-EDR sample have strong MgII and FeII, but have $W_0^{\lambda 2796} \lesssim 1.0$ Å; these belong in sub-sample 3. As we will see in §4.2, this classification is necessary for determining the incidence, $n_{DLA}(z)$, of the DLAs.

3. THE DLAS

Here we present Voigt profile fits to the new DLAs. These 28 systems, 3 of which were observed in HST-Cycle 9, are shown in Figure 1. The resulting column densities and errors are listed in Table 1. As is usually the case for high column density lines, the Ly α forest populates DLA troughs making it inappropriate to use an automated routine such as least squares minimization to fit a Voigt profile to the data. Therefore, the best fit was estimated using the following procedure. Since the continuum fit is the largest source of uncertainty in determining $N(HI)$, errors were determined by moving the continuum level by 1σ above and below the best-fit continuum, renormalizing the spectrum, and refitting a Voigt profile (see RT00). The differences between these values and $N(HI)$ determined from the best-fit continuum are listed as the positive and negative errors in column 10 of Table 1.

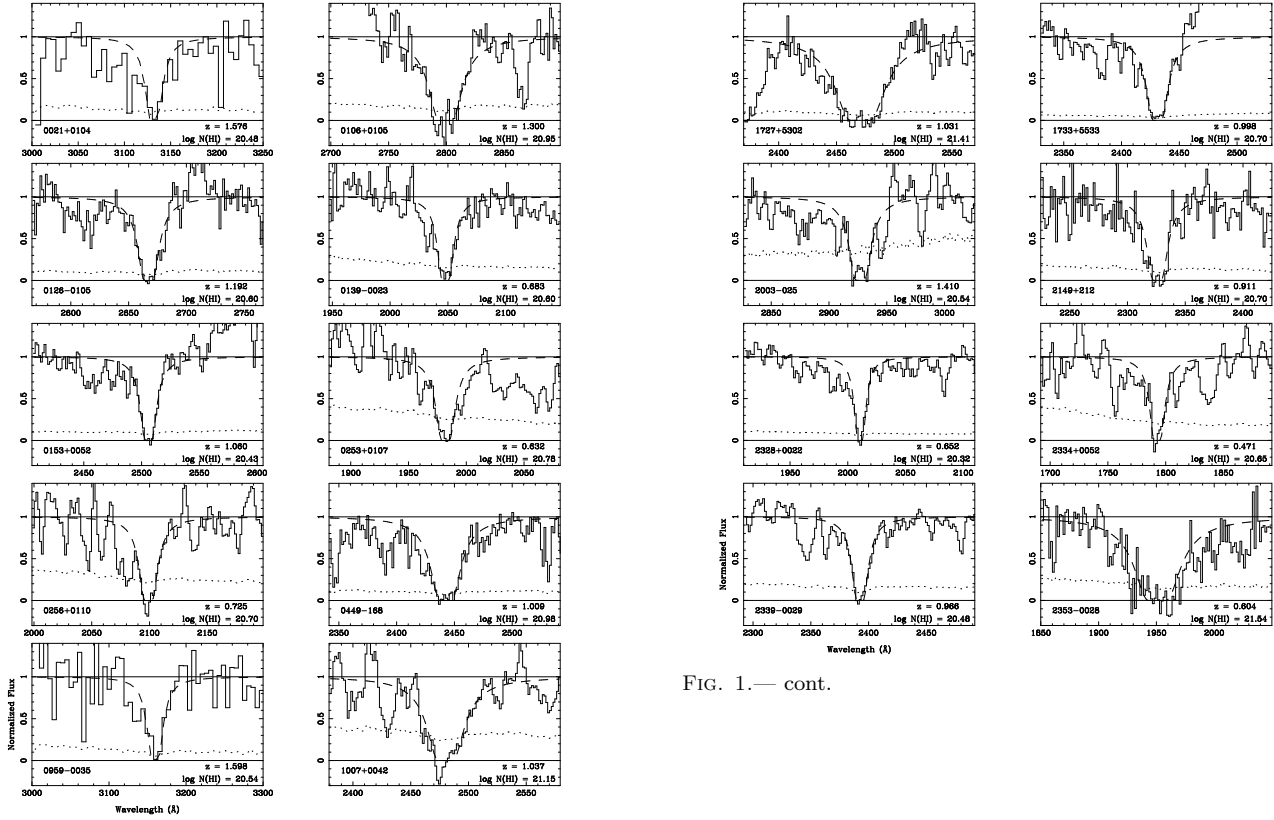


FIG. 1.— cont.

FIG. 1.— Voigt profile fits to the DLA lines. The quasar, MgII z_{abs} , and $N(HI)$ are given in each panel. The dashed line is the best-fit Voigt profile and the dotted line is the 1σ error array.

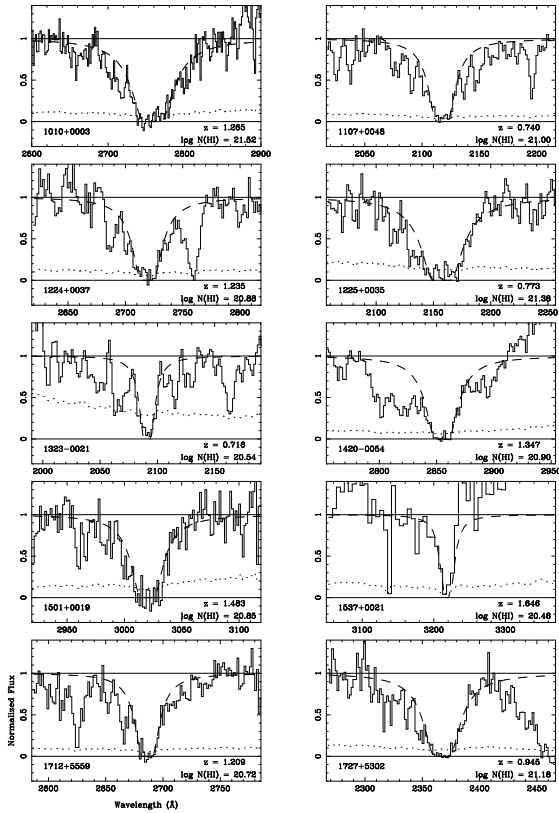


FIG. 1.— cont.

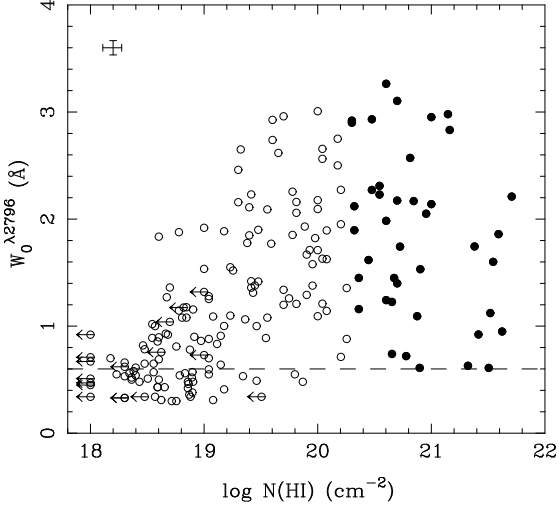


FIG. 2.— Plot of $W_0^{\lambda 2796}$ vs. $\log N(HI)$. Filled circles are DLAs with $N(HI) \geq 2 \times 10^{20}$ atoms cm^{-2} . Arrows are upper limits in $N(HI)$. Typical uncertainties are given by the error bars in the top left corner.

4. STATISTICAL RESULTS

4.1. Parameter Distributions and Correlations

Since the systems in our sample were selected based on the rest equivalent width of MgII $\lambda 2796$, measurements of $W_0^{\lambda 2796}$ and $N(HI)$ exist for all 197 systems. MgII $\lambda 2803$, the weaker member of the doublet, was also measured for all systems; measurements of the FeII $\lambda 2600$ and MgI $\lambda 2852$ lines were possible only for a subset. In this section, we explore correlations among metal line REWs and HI column density. Figure 2 is a plot of $W_0^{\lambda 2796}$ versus $\log N(HI)$. We note that the upper left region of the figure is not populated, implying that systems with $W_0^{\lambda 2796} > 2.0 \text{ \AA}$ always have HI column densities $N(HI) > 1 \times 10^{19} \text{ cm}^{-2}$. Figure 3 gives the distribution of MgII $W_0^{\lambda 2796}$; the DLAs form the shaded histogram. It is noteworthy that there are no DLAs with $W_0^{\lambda 2796} < 0.6 \text{ \AA}$.⁶ In addition, the fraction of systems that are DLAs increases with increasing $W_0^{\lambda 2796}$. This is shown as a histogram in Figures 4 and 5; the y-axis on the left gives the fraction of DLAs as a function of $W_0^{\lambda 2796}$. We also plot the mean HI column density in each bin as solid circles with the scale shown on the right. Upper limits are assumed to be detections.⁷ Figure 4 includes all observed MgII systems and Figure 5 includes only the DLAs. The vertical error bars are standard deviations in the mean and are due to the spread of $N(HI)$ values in each bin, and the horizontal error bars indicate bin size. For the MgII systems there is a dramatic increase of a

⁶ Only one known DLA has a lower metal-line REW. The 21 cm absorber at $z = 0.692$ towards 3C 286 has $W_0^{\lambda 2796} = 0.39 \text{ \AA}$ and $W_0^{\lambda 2600} = 0.22 \text{ \AA}$ (Cohen et al. 1994). However, none of the 21 cm absorbers are included in our analysis because they are biased systems with respect to the determination of DLA statistics (see RT00).

⁷ The two systems with high b values (the $z_{abs} = 1.6101$ system towards 1329+412 and the $z_{abs} = 1.2528$ system towards 1821+107) are included in the histograms because it is clear that they are not DLAs. However, since their HI column density is not known, they are not included in the calculation of the mean column density.

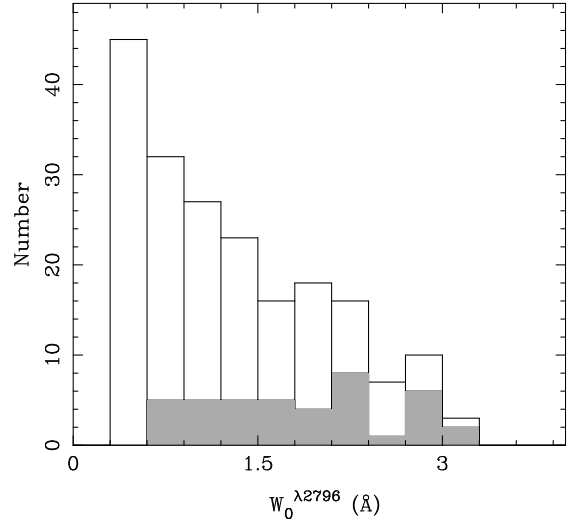


FIG. 3.— Distribution of MgII $\lambda 2796$ rest equivalent widths, $W_0^{\lambda 2796}$. The shaded histogram represents systems that are DLAs. Note that there are no DLAs in the first bin, i.e., for MgII $W_0^{\lambda 2796} < 0.6 \text{ \AA}$. The fraction of DLAs increases with increasing $W_0^{\lambda 2796}$ for $W_0^{\lambda 2796} \geq 0.6 \text{ \AA}$.

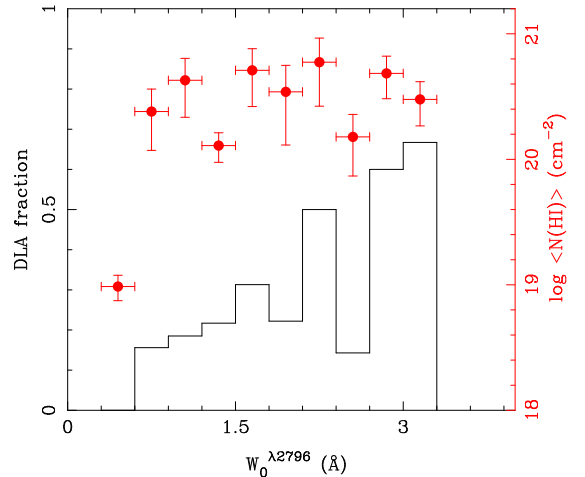


FIG. 4.— The histogram shows the fraction of MgII systems that are DLAs as a function of MgII $W_0^{\lambda 2796}$, with the scale shown on the left axis. The solid circles are the logarithm of the mean HI column density in each bin. The scale is shown on the right.

factor of ≈ 36 in the mean HI column density from the first to the second bin, beyond which $\langle N(HI) \rangle$ remains constant within the errors. In particular, Figure 4 shows that for our sample the probability of a MgII system being a DLA is $P \approx 0$ for $W_0^{\lambda 2796} < 0.6 \text{ \AA}$ and, assuming a linear dependence, $P \approx 0.16 + 0.18(W_0^{\lambda 2796} - 0.6)$ for $0.6 \leq W_0^{\lambda 2796} < 3.3 \text{ \AA}$. For systems with $0.3 \text{ \AA} \leq W_0^{\lambda 2796} < 0.6 \text{ \AA}$, $\langle N(HI) \rangle = (9.7 \pm 2.2) \times 10^{18} \text{ cm}^{-2}$, and $\langle N(HI) \rangle = (3.5 \pm 0.7) \times 10^{20} \text{ cm}^{-2}$ for systems with $W_0^{\lambda 2796} \geq 0.6 \text{ \AA}$. Figure 5 shows a trend for decreasing DLA column density with $W_0^{\lambda 2796}$. The reasons for this are not obvious, but are likely to be due to small number statistics (see Figure 2), a real physical effect, or a selection effect that is not yet understood (see Turnshek et al. 2005, §5.1).

Since some of the higher $W_0^{\lambda 2796}$ systems in the sam-

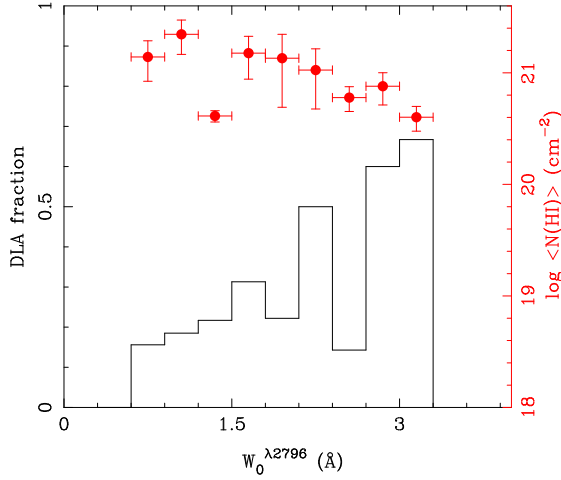


FIG. 5.— Same as Figure 4, but points are for DLAs only.

ple have an FeII λ 2600 selection criterion folded in, we repeat the above analysis here for the non-FeII selected part of the sample. Figure 6 is a $W_0^{\lambda 2796}$ distribution for systems that do not include the FeII selection criterion. These are systems that belong to sub-samples 1 and 2. The DLAs form the shaded histogram. The first bin contains the same systems as in Figure 3. Even with this smaller sample, 111 systems compared to 197, we find that the fraction of DLAs increases with $W_0^{\lambda 2796}$. The mean HI column density for this sample is shown in Figure 7. Since the number of systems in the higher $W_0^{\lambda 2796}$ bins is small, we bin the data differently from Figure 4 and, for comparison, show the Figure 4 sample rebinned as well. We find that the FeII selection has no effect on the mean column density as a function of $W_0^{\lambda 2796}$. Consistent with our larger sample, for systems with $W_0^{\lambda 2796} \geq 0.6 \text{ \AA}$ we find $\langle N(HI) \rangle = (3.40 \pm 1.25) \times 10^{20} \text{ cm}^{-2}$. One might expect that since the fraction of DLAs increases with increasing $W_0^{\lambda 2796}$ and that the FeII selection primarily affects higher $W_0^{\lambda 2796}$ systems, the mean HI column density should be higher in the FeII selected sample. However, again, this may be offset by the fact that the mean DLA HI column density decreases with increasing $W_0^{\lambda 2796}$, thus keeping the mean HI column density of FeII and non-FeII selected samples indistinguishable.

Figure 8 is a plot of $W_0^{\lambda 2796}$ vs. $W_0^{\lambda 2600}$ for systems with measured values of $W_0^{\lambda 2600}$, including upper limits. In RT00 we found that $50(\pm 16)\%$ of the 20 systems (excluding upper limits and 21 cm absorbers) with $W_0^{\lambda 2796} > 0.5 \text{ \AA}$ and $W_0^{\lambda 2600} > 0.5 \text{ \AA}$ are DLAs. Now, with the expanded sample that includes 106 systems in this regime, we find that $36(\pm 6)\%$ are DLAs. The dashed line is a least-squares fit with slope $b = 1.36 \pm 0.08$ and intercept $a = 0.24 \pm 0.06$. It was determined using the BCES estimator of Akritas & Bershady (1996), assuming intrinsic scatter but uncorrelated errors in $W_0^{\lambda 2796}$ and $W_0^{\lambda 2600}$. Upper limits were not used for the fit. We note that DLAs do not populate the top left region of the diagram where the $W_0^{\lambda 2796}$ to $W_0^{\lambda 2600}$ ratio is $\gtrsim 2$. In fact, if the sample is restricted to systems with $W_0^{\lambda 2796}/W_0^{\lambda 2600} < 2$, all but one of the DLAs in Figure 8 are retained, the outliers in the top left region are excluded as are most sys-

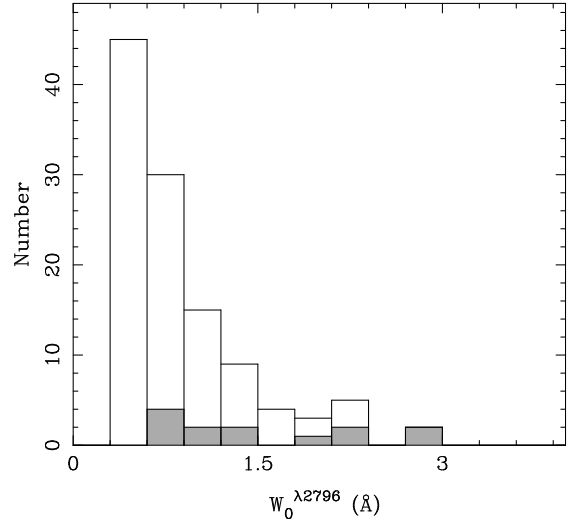


FIG. 6.— Same as Figure 3 but for non-FeII selected systems. These form sub-samples 1 and 2. The shaded histogram shows the DLAs. As in Figure 3, the fraction of DLAs in bins with $MgII W_0^{\lambda 2796} \geq 0.6 \text{ \AA}$ increases with increasing $W_0^{\lambda 2796}$.

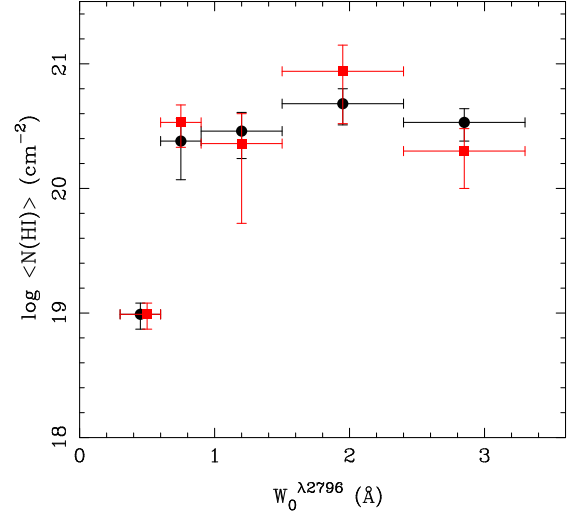


FIG. 7.— Logarithm of the mean HI column density of absorbers as a function of $MgII W_0^{\lambda 2796}$. The red solid squares are for non-FeII selected systems, i.e., for sub-samples 1 and 2. The black solid circles are the same data shown in Fig. 4, but rebinned to match the binning of the sub-sample without FeII selection. The data points in the first bin are identical but have been displaced for clarity. The FeII selection has no effect on the mean HI column density as a function of $MgII W_0^{\lambda 2796}$.

tems in the lower left corner of the plot. Figure 9 shows this truncated sample; the slope of the least-squares fit does not change significantly. We find $b = 1.43 \pm 0.08$ and $a = 0.01 \pm 0.08$ for this definition of the sample. The only DLA that has been eliminated is the one with the smallest value of $W_0^{\lambda 2600}$. However, given the measurement errors for this system, its $W_0^{\lambda 2796}/W_0^{\lambda 2600}$ ratio is within 1σ of 2. The implication is that a system with metal line ratio $W_0^{\lambda 2796}/W_0^{\lambda 2600} > 2$ has nearly zero probability of being a DLA. For this truncated sample with $W_0^{\lambda 2796}/W_0^{\lambda 2600} < 2$, but no restrictions on the individual values of $W_0^{\lambda 2796}$ or $W_0^{\lambda 2600}$, $38(\pm 6)\%$ are DLAs. In addition, all known 21 cm absorbers, including the

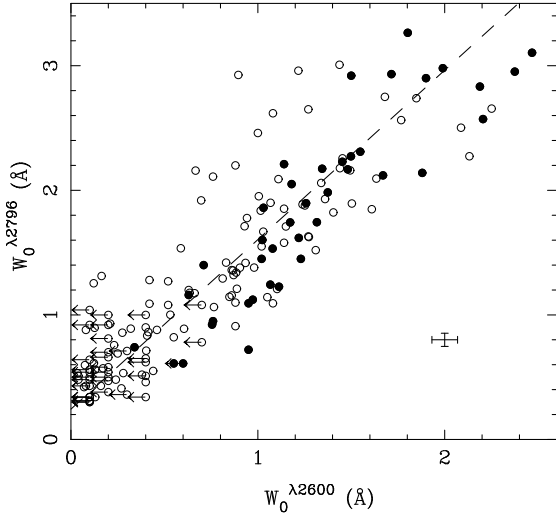


FIG. 8.— Plot of $W_0^{\lambda 2796}$ vs. $W_0^{\lambda 2600}$ for all MgII systems that have measured values of $W_0^{\lambda 2600}$. Filled circles are DLAs. Typical error bars are shown at lower right. The dashed line is the best fit linear correlation described in the text with slope $b = 1.36$.

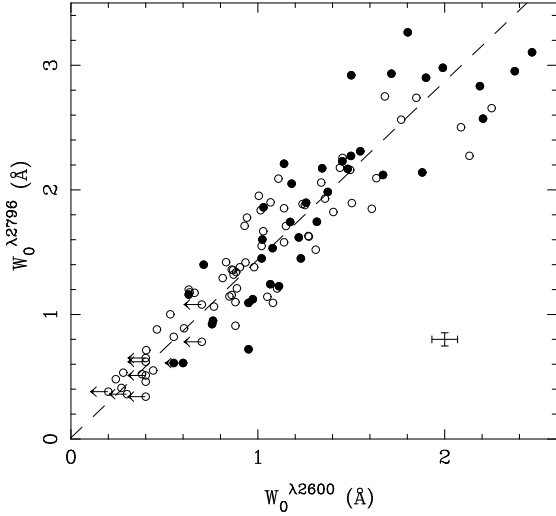


FIG. 9.— Plot of $W_0^{\lambda 2796}$ vs. $W_0^{\lambda 2600}$ for systems with $W_0^{\lambda 2796}/W_0^{\lambda 2600} < 2$. Filled circles are DLAs. Non-DLAs in the upper left and lower left region of the diagram have been eliminated and the correlation is tighter than what is seen in Figure 8. Also, 38% of all systems are DLAs regardless of the values of $W_0^{\lambda 2796}$ and $W_0^{\lambda 2600}$; we believe this to be a more robust predictor of the presence of DLAs in MgII-FeII systems. The slope of the best fit linear correlation is $b = 1.43$.

$z = 0.692$ system towards 3C 286 mentioned above, have $W_0^{\lambda 2796}/W_0^{\lambda 2600} < 2$. Thus, the $W_0^{\lambda 2796}/W_0^{\lambda 2600}$ ratio provides a more robust predictor of the presence of a DLA.

This result is shown more dramatically in Figures 10 and 11. The ratio $W_0^{\lambda 2796}/W_0^{\lambda 2600}$ is plotted as a function of $N(HI)$ in Figure 10. Ratios above 5 are not shown for clarity. These are mainly confined to $\log N(HI) < 19.2$ with only one system above this column density at $\log N(HI) = 19.6$. The DLAs populate the region of the plot where $1 \lesssim W_0^{\lambda 2796}/W_0^{\lambda 2600} \lesssim 2$; the two outliers lie within 1σ of this range. A plot of the ratio $W_0^{\lambda 2796}/W_0^{\lambda 2600}$ vs. $W_0^{\lambda 2852}$ for systems with mea-

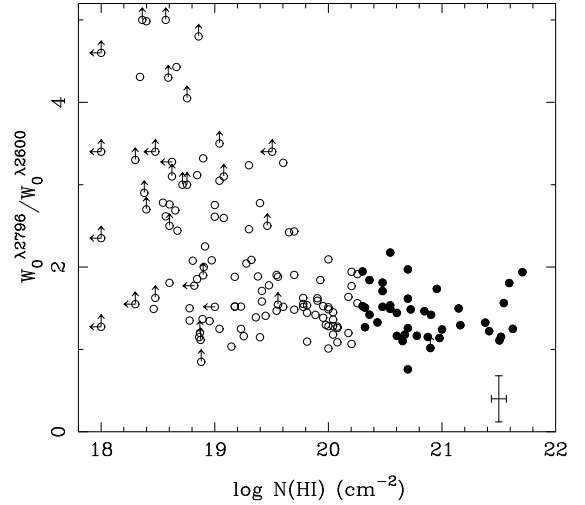


FIG. 10.— Plot of $W_0^{\lambda 2796}/W_0^{\lambda 2600}$ vs. $N(HI)$. Systems with $W_0^{\lambda 2796}/W_0^{\lambda 2600} > 5$ are not shown for clarity; all of these have $\log N(HI) < 19.6$. The DLAs (filled circles) are confined to the region of the plot where $1 \lesssim W_0^{\lambda 2796}/W_0^{\lambda 2600} \lesssim 2$.

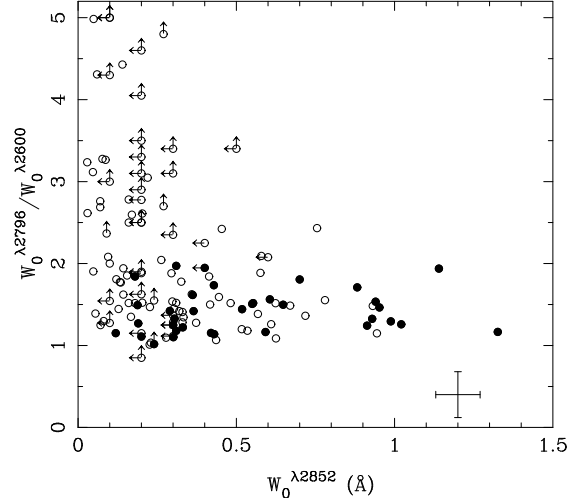


FIG. 11.— Plot of $W_0^{\lambda 2796}/W_0^{\lambda 2600}$ vs. MgI $W_0^{\lambda 2852}$. Filled circles are DLAs. Typical error bars are shown in the lower right corner. Again, the DLAs are confined to the region where $1 \lesssim W_0^{\lambda 2796}/W_0^{\lambda 2600} \lesssim 2$, but span almost the entire range of $W_0^{\lambda 2852}$ ($W_0^{\lambda 2852} > 0.1 \text{ \AA}$).

sured values of $W_0^{\lambda 2852}$, including upper limits, is shown in Figure 11. Again, the DLAs are confined to the region where $1 \lesssim W_0^{\lambda 2796}/W_0^{\lambda 2600} \lesssim 2$, but span almost the entire range of $W_0^{\lambda 2852}$ ($W_0^{\lambda 2852} > 0.1 \text{ \AA}$). The two systems outside the range $1 \lesssim W_0^{\lambda 2796}/W_0^{\lambda 2600} \lesssim 2$ from Figure 10 do not have information on $W_0^{\lambda 2852}$. Of the systems with measured values of $W_0^{\lambda 2852}$, 32 of the 77 systems with $W_0^{\lambda 2796}/W_0^{\lambda 2600} \lesssim 2$ and $W_0^{\lambda 2852} \geq 0.1$, i.e., $42(\pm 7)\%$, are DLAs. The other 9 DLAs either do not have measured values of $W_0^{\lambda 2852}$, or have high upper limits due to poor data quality. We also find that 9 out of the 11 systems with $W_0^{\lambda 2852} > 0.8 \text{ \AA}$ are DLAs. We note that systems with $W_0^{\lambda 2796}/W_0^{\lambda 2600} \gtrsim 2$ are likely to have low values of $W_0^{\lambda 2852}$.

For completeness, we also plot $W_0^{\lambda 2600}$ vs. $\log N(HI)$

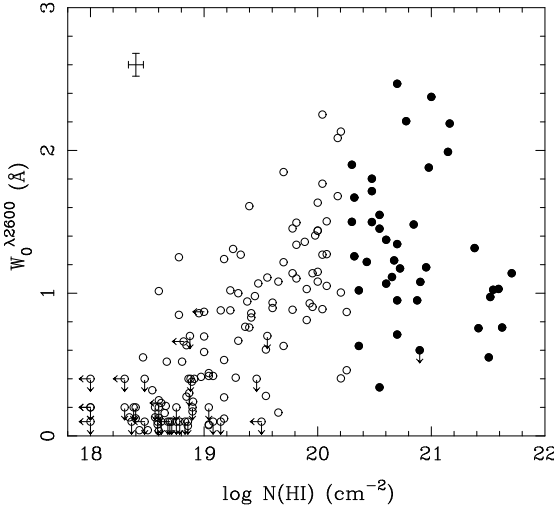


FIG. 12.— Plot of $W_0^{\lambda 2600}$ vs. $\log N(HI)$. Arrows indicate upper limits. Filled circles are DLAs. Typical uncertainties are given by the error bars in the top left corner.

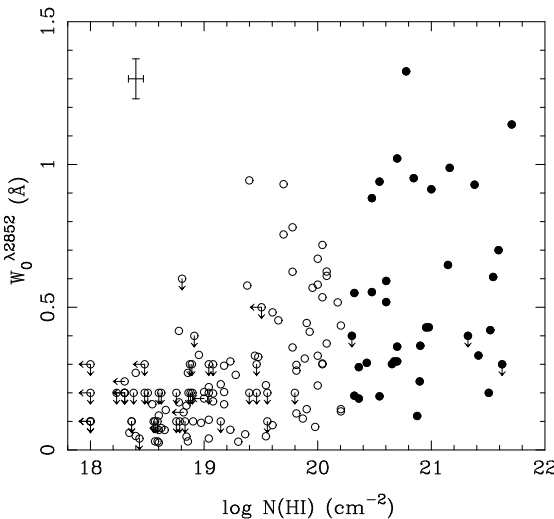


FIG. 13.— Plot of $W_0^{\lambda 2852}$ vs. $\log N(HI)$. Arrows indicate upper limits. Filled circles are DLAs. Typical uncertainties are given by the error bars in the top left corner.

in Figure 12 and $W_0^{\lambda 2852}$ vs. $\log N(HI)$ in Figure 13. There is no obvious trend in these distributions except for the fact that the upper left regions of the plots are not populated. There are no high REW, low HI column density systems. This is not a selection effect since column densities as low as 10^{18} cm^{-2} can often be easily measured. This implies that systems with $W_0^{\lambda 2600} \gtrsim 1 \text{ \AA}$ or $W_0^{\lambda 2852} \gtrsim 0.5 \text{ \AA}$ generally have HI column densities $N(HI) > 10^{19.0} \text{ cm}^{-2}$. Below this fairly sharp boundary, metal-line REWs span all values of HI column density.

4.1.1. Discussion

How can these trends be interpreted? Apart from the upper envelopes in Figures 2, 12, and 13, there is no other simple correlation between metal-line rest equivalent width and HI column density. Since the metal lines are saturated, the rest equivalent width is more a measure of velocity spread, not column density. High resolution observations of MgII absorption lines have shown

that the stronger systems break up into many components (e.g., Churchill, Vogt, & Charlton 2003), and span velocity intervals of up to 400 km/s. Turnshek et al. (2005) show line equivalent widths in velocity units of $\gtrsim 800 \text{ km/s}$ in the strongest systems found in the SDSS. These highest equivalent width systems may arise in galaxy groups; however, the more common systems like those in our DLA survey are more likely to arise in clouds that are bound in galaxy-sized potentials. A DLA is observed if at least one of the clouds along the sightline happens to be cold (less than a 100 K), and with a velocity dispersion of a few 10s of km/s. A simple interpretation is that the greater the number of clouds along the sightline, the higher the probability of encountering a DLA. This would explain the higher fraction of DLAs among large $W_0^{\lambda 2796}$ systems and the lack of a correlation between $W_0^{\lambda 2796}$ and $N(HI)$ other than the upper envelopes in Figures 2, 12, and 13. Only rarely would a sightline intersect a single cloud resulting in small $W_0^{\lambda 2796}$ and high $N(HI)$, as in the 3C 286 system described in §4.1. This probabilistic approach to explain metal-line and HI strengths in high- $N(HI)$ absorbers was also proposed by Briggs & Wolfe (1983) to explain their MgII survey for 21 cm absorbers. They proposed a two-phase model where the 21 cm absorption is produced in galaxy disks, and the metal-line components that do not produce 21 cm absorption are produced in galactic halos. However, this multi-component/cloud model is likely to be valid in any gas-rich galaxy, as is evidenced by DLA galaxy imaging studies (Le Brun et al. 1997; Rao & Turnshek 1998; Turnshek et al. 2001; Rao et al. 2003; Turnshek et al. 2004). The disk models of Prochaska & Wolfe (1997) and the Haehnelt, Steinmetz, & Rauch (1998) models of infalling and merging clouds could reproduce these observations equally well. In other words, DLAs arise in pockets of cold gas embedded within warm diffuse gas or gas clouds in any bound system.

Twenty one cm observations of low-redshift DLAs also reveal some cloud structure. For example, the $z = 0.313$ system towards PKS 1127–145 shows 5 components and the $z = 0.394$ system towards B0248+430 is resolved into 3 components (Lane 2000; Lane & Briggs 2001; Kanekar & Chengalur 2001). Since the MgII line for these systems has not been observed at a resolution as high as the 21 cm observations, a one-to-one correspondence between the metal-line and 21 cm clouds cannot be drawn. In other instances, both warm and cold gas have been detected in a 21 cm DLA; Lane, Briggs, & Smette (2000) find that two-thirds of the column density in the $z = 0.0912$ DLA towards B0738+313 is contained in warm phase gas, and the rest is contained in two narrow components. The $z = 0.2212$ absorber towards the same quasar was also found to exhibit similar characteristics (Kanekar, Ghosh, & Chengalur 2001). In each of these cases, the line of sight probably intersects two cold clouds in addition to warm diffuse gas spread over a wider range of velocities that can be detected only in 21 cm observations of very high sensitivity. There are also several instances of DLAs not being detected at 21 cm (Kanekar & Chengalur 2003). High spin temperatures ($T_s \gtrsim 1000 \text{ K}$) corresponding to warm diffuse gas and/or covering factors less than unity towards extended quasar radio components have been suggested as possible

explanations (Kanekar & Chengalur 2003; Curran et al. 2005).

Clearly, a wide variety of cloud properties and their combinations are responsible for the observed properties of MgII, DLA, and 21 cm absorption lines. Large simulations of galaxy sightlines with varying cloud properties that reproduce the metal-line versus DLA correlations shown in Figures 2-13 would be an important next step towards improving our understanding of these absorption line systems. The simulations should not only be able to reproduce the frequency of occurrence of DLAs in MgII systems, but also the number density evolution of MgII systems and DLAs. Moreover, further analysis on large data sets might enable us to predict the occurrence of DLAs among metal-line systems and determine their HI column densities to some degree of accuracy, but this is a project for future study. For the remainder of this paper we discuss the statistical properties of neutral gas in the low redshift universe as derived from the expanded HST sample.

4.2. Redshift number density n_{DLA}

The redshift number density of DLAs, n_{DLA} , sometimes written as dn/dz , can be determined using the equation

$$n_{DLA}(z) = \eta(z) n_{MgII}(z), \quad (1)$$

where $\eta(z)$ is the fraction of DLAs in a MgII sample as a function of redshift and $n_{MgII}(z)$ is the redshift number density of MgII systems. Since our MgII sample was assembled under various selection criteria (see §2), $n_{MgII}(z)$ needs to be evaluated carefully. We can express $n_{MgII}(z)$ for our sample as

$$n_{MgII}(z) = \frac{1}{197} \sum_i w_i n_{MgII_i}(z), \quad (2)$$

where the sum is over all 197 systems, w_i is a weighting factor that depends on the i^{th} system's selection criterion for being included in the survey, and $n_{MgII_i}(z)$ is the i^{th} system's dn/dz value calculated using the parametrization derived in the Appendix of NTR05:

$$dn/dz = N^* (1+z)^\alpha e^{-\frac{W_0}{W^*}(1+z)^{-\beta}}, \quad (3)$$

where we have retained the notation given in NTR05 and $W \equiv W_0^{\lambda 2796}$. N^* , W^* , α , and β are constants. This expression is an integral over all $W_0^{\lambda 2796}$ greater than W_0 . For our calculation, W_0 is different for each of four sub-samples that comprise our total sample (see §2 and Table 1). Thus, for example, a system that belongs to sub-sample 1 has a REW threshold $W_0 = 0.3$ Å in Equation 3 and weight $w_i = 1$ in Equation 2, while a system in sub-sample 2 has $W_0 = 0.6$ and $w_i = 1$. This is because sub-samples 1 and 2 are purely MgII-selected samples with no regard to the strength or presence of the FeII $\lambda 2600$ line. On the other hand, a system that belongs to sub-sample 3 has $W_0 = 0.6$ in Equation 3 and weight $w_i = 0.54$ in Equation 2. This is because an FeII $\lambda 2600$ criterion was used to select the system in addition to $W_0^{\lambda 2796}$, and 54% of the 1,130 $W_0^{\lambda 2796} \geq 0.6$ Å systems in the MgII survey of NTR05 have $W_0^{\lambda 2600} \geq 0.5$ Å. Similarly, for systems in sub-sample 4, $W_0 = 1.0$ and $w_i = 0.72$. In this case, 72% of the 781 $W_0^{\lambda 2796} \geq 1.0$ Å systems in NTR05 have $W_0^{\lambda 2600} \geq 0.5$ Å. For sub-samples

3 and 4 we have assumed that the fraction of MgII systems that are also strong FeII systems is independent of redshift.

The MgII doublet moves out of the SDSS spectroscopic range for redshifts $z < 0.36$. In order to extend MgII statistics to lower redshifts, we conducted a survey of quasars with the Multiple Mirror Telescope (MMT) on Mount Hopkins, AZ (Nestor, 2004). These results, which will be presented in a forthcoming paper (Nestor, Turnshek, & Rao 2006, in preparation), were used to determine DLA statistics for the redshift range $0.11 \leq z \leq 0.36$ using the same procedure described above. Of the 11 systems from our sample in this redshift range, nine belong in sub-sample 1 and two are in sub-sample 2.

Figure 14 shows the results for $n_{DLA}(z)$ at low redshift split into two redshift bins (solid squares). We find 18 DLAs in 104 MgII systems in the redshift interval $0.11 < z \leq 0.9$ with $n_{DLA}(z = 0.609) = 0.079 \pm 0.019$ and 23 DLAs in 94 MgII systems in the redshift interval $0.9 < z \leq 1.65$ with $n_{DLA}(z = 1.219) = 0.120 \pm 0.025$. We did not find it necessary to apply a Malmquist bias correction for the number of systems with $N(HI) \geq 2 \times 10^{20}$ cm $^{-2}$ (as was done in RT00) because the sample contains an equal number of systems within 1σ above and below this threshold value. Standard error propagation procedures were used to determine uncertainties. The points are plotted at the mean redshift of the MgII samples. The high-redshift data points are from Prochaska & Herbert-Fort (2004) and the $z = 0$ point was estimated by Zwaan et al. (2005a) from a WSRT survey of HI in the local universe. The solid curve is a no-evolution curve in the standard Λ CDM cosmology that we refer to as the “737” cosmology where $(h, \Omega_M, \Omega_\Lambda) = (0.7, 0.3, 0.7)$. This curve, which has been normalized at the $z = 0$ data point, shows that the comoving cross section for DLA absorption declined rapidly by a factor of ≈ 2 until $z \approx 2$ and has remained constant since then. This behavior might be a consequence of what has been observed in other studies of galaxy evolution, namely, that today's galaxies were in place by $z \approx 1$ and are a consequence of rapid merger and/or collapse events that occurred prior to this epoch.

It has been customary in quasar absorption line studies to plot the logarithm of the redshift number density in order to illustrate its power law dependence with redshift, i.e., $n(z) = n_0(1+z)^\gamma$. In $\Lambda = 0$ cosmologies, the exponent is a measure of evolution. For example, $\gamma = 1$ for $q_0 = 0$ or $\gamma = 0.5$ for $q_0 = 0.5$ implies no intrinsic evolution of the absorbers. Any significant departure from these values for γ was considered as evidence for evolution in the product of the comoving number density and cross section of absorbers. We plot $\log n_{DLA}(z)$ as a function of $\log(1+z)$ in Figure 15. The straight line is the power law fit to the data points with slope $\gamma = 1.27 \pm 0.11$, and the curve is the same no-evolution function shown in Figure 14. Thus, in the past, the observations would have been interpreted as being consistent with the DLA absorbers undergoing no intrinsic evolution in a $q_0 = 0$ universe, and marginally consistent with evolution in a $q_0 = 0.5$ universe. With the now widely accepted concordance cosmology, the interpretation has changed quite dramatically; as noted above, the nature of the evolution is redshift dependent.

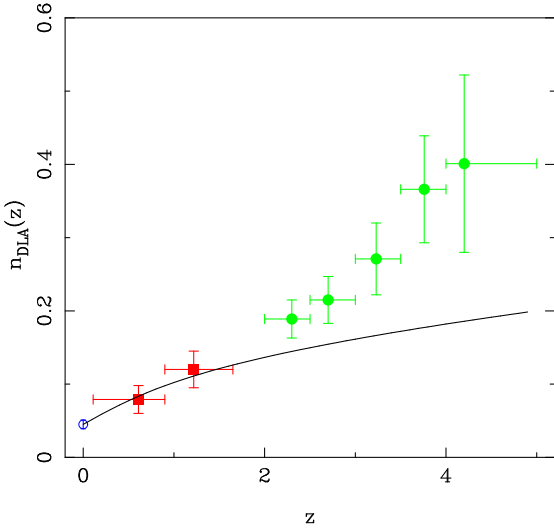


FIG. 14.— Plot of $n_{DLA}(z)$ versus redshift. The new low-redshift data points are shown as filled squares. The high-redshift points (filled circles) are from Prochaska & Herbert-Fort (2004) and the $z = 0$ data point is from an analysis of local HI using the WSRT (Zwaan et al. 2005a). The solid line is a no-evolution curve in a standard “737” Λ CDM cosmology with $(h, \Omega_M, \Omega_\Lambda) = (0.7, 0.3, 0.7)$ normalized at the $z = 0$ data point. This curve implies that the comoving cross section for absorption declined rapidly by a factor of ≈ 2 until $z \approx 2$ and has remained constant since then. This is consistent with the idea that today’s structures have been in place since $z \approx 1$ and are a consequence of merger events that occurred prior to this epoch.

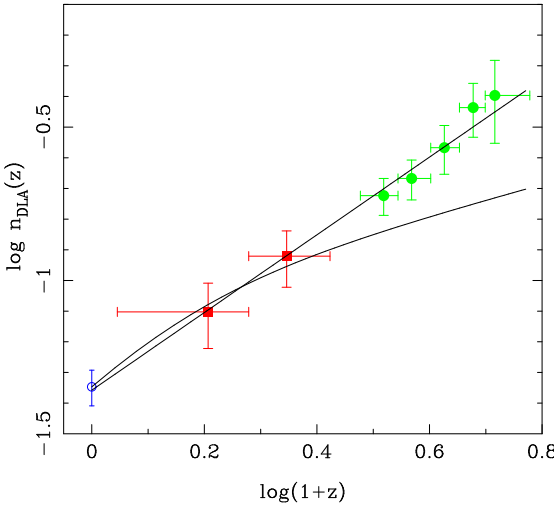


FIG. 15.— Plot of $\log n_{DLA}(z)$ as a function of $\log(1+z)$. The straight line is the power law fit to the data points with slope $\gamma = 1.27 \pm 0.11$, and the curve is the no-evolution function shown in Figure 14.

Further implications of this evolution are discussed in §5 along with inferences drawn from the evolution in Ω_{DLA} (§4.3) and the HI column density distribution (§4.4).

4.3. Cosmological mass density Ω_{DLA}

We can determine Ω_{DLA} from the DLA column densities listed in Table 1 and $n_{DLA}(z)$ via the expression

$$\Omega_{DLA}(z) = \frac{\mu m_H H_0}{c \rho_c} n_{DLA}(z) \langle N(HI) \rangle \frac{E(z)}{(1+z)^2}, \quad (4)$$

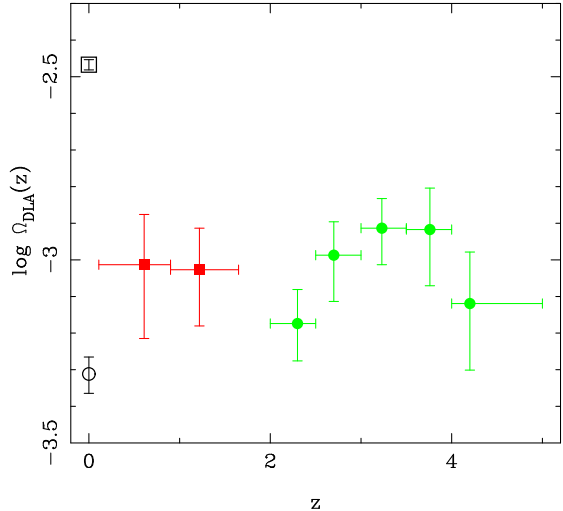


FIG. 16.— Cosmological mass density of neutral gas, Ω_{DLA} , as a function of redshift. The filled squares are the new low-redshift data points. The high-redshift points (filled circles) are from Prochaska & Herbert-Fort (2004) and the open circle at $z = 0$ is from Zwaan et al. (2005b). The open square at $z = 0$ is the mass density in stars estimated by Panter, Heavens, & Jimenez (2004) from the SDSS. While the statistics have improved considerably, our basic conclusion from RT00 has remained unchanged, namely, that the cosmological mass density of neutral gas has remained constant from $z \approx 5$ to $z \approx 0.5$.

where

$$E(z) = \frac{H(z)}{H_0} = [\Omega_M(1+z)^3 + (1-\Omega_M-\Omega_\Lambda)(1+z)^2 + \Omega_\Lambda]^{1/2}. \quad (5)$$

Again, the “737” cosmology has been used in the calculation of Ω_{DLA} . Also, $\mu = 1.3$ corrects for a neutral gas composition of 75% H and 25% He by mass, m_H is the mass of the hydrogen atom, ρ_c is the critical mass density of the universe, and $\langle N(HI) \rangle$ is the mean HI column density of DLAs in each bin.

In contrast to the redshift number density evolution shown in Figure 14, we find that Ω_{DLA} has remained constant from $z = 5$ to $z = 0.5$ to within the uncertainties. Figure 16 shows the new results as solid squares. Specifically, for the redshift range $0.11 < z \leq 0.90$, we find $\langle N(HI) \rangle = (1.27 \pm 0.36) \times 10^{21} \text{ cm}^{-2}$ and $\Omega_{DLA}(z = 0.609) = (9.7 \pm 3.6) \times 10^{-4}$, and for the range $0.90 < z < 1.65$ we get $\langle N(HI) \rangle = (1.07 \pm 0.23) \times 10^{21} \text{ cm}^{-2}$ and $\Omega_{DLA}(z = 1.219) = (9.4 \pm 2.8) \times 10^{-4}$. The uncertainties have been reduced considerably in comparison to our results in RT00. The reasons for this are two fold. First, the uncertainty in n_{MgII} has been significantly reduced due to the fact that the MgII sample size was increased 10-fold. Second, the number of DLAs in each bin has increased by more than a factor of 3. Thus, the uncertainties in the low- and high-redshift data points are now comparable. Note that the statistics of the high-redshift data are also improved due to the inclusion of an SDSS DLA sample (Prochaska & Herbert-Fort 2004). Nevertheless, our basic conclusion from RT00 has remained unchanged, namely, that the cosmological mass density of neutral gas remains roughly constant from $z \approx 5$ to $z \approx 0.5$. The drop in redshift number density from $z = 5$ to $z = 2$ along with a constant mass density in this range indicates that while the product

of galaxy cross section and comoving number density is declining, the mean column density per absorber is increasing. This is, again, consistent with the assembly of higher density clouds as galaxy formation proceeds.

On the other hand, a constant cross section from $z \approx 1$ to $z = 0$ along with a drop in mass density from $z \approx 0.5$ to $z = 0$ is indicative of star formation that depletes the highest column density gas while keeping the absorption cross section constant. This would in turn require that the column density distribution of DLAs change such that the ratio of high to low column densities decreases from low-redshift to $z = 0$. As we will see in the next section, the column density distribution does show some evidence for this.

4.4. Column density distribution $f(N)$

Figure 17 shows the normalized cumulative column density distribution (CDD) for the three redshift regimes. The dashed curve is the $z = 0$ CDD from an analysis of an HI diameter-limited sample of local galaxies from Rao & Briggs (1993) while the dotted curve is the $z = 0$ distribution derived by Ryan-Weber et al. (2003, henceforth R-W03; 2005) from HIPASS data. The thick, solid curve is derived from the DLAs in Table 1 and the thin, solid curve is from the “total” sample of Prochaska & Herbert-Fort (2004). The change in the three CDDs with redshift is exactly what is expected based on the n_{DLA} and Ω_{DLA} results. Namely, that the low-redshift CDD shows a higher incidence of high column density systems than at high redshift presumably due to the assembly of gas as galaxy formation proceeds, followed by a decrease in the fraction of high column density systems to $z = 0$, presumably due to the depletion of gas during star formation. Thus, at least qualitatively, the evolutionary behavior of n_{DLA} , Ω_{DLA} , and the CDD are entirely consistent with one another. A KS test shows that there is a 25% probability that the high- and low-redshift curves are drawn from the same population; this is significantly higher than what we observed in RT00, where the two samples had only a 2.8% probability of being drawn from the same population. However, the general trend that the low-redshift sample has a higher fraction of high column density system still remains.

The absolute CDD can be determined using the equation

$$f(N, z) = n_{DLA}(z) \frac{E(z)}{(1+z)^2} \frac{y(N, z)}{\Delta N} \quad (6)$$

where $y(N, z)$ is the fraction of DLAs with column densities between N and $N + \Delta N$ at redshift z , and $E(z)$ is as given in Equation 5. Figure 18 is a plot of the log of the absolute CDD function, $\log f(N)$, as a function of $\log N(HI)$. The turnover with redshift is most apparent in the lowest and highest column density bins. We derive $\beta = 1.4 \pm 0.2$ and $\beta = 1.8 \pm 0.1$ at low and high redshift respectively, where the CDD is expressed as $f(N) = BN^{-\beta}$. At $z = 0$, R-W03 derive $\beta = 1.4 \pm 0.2$ for $\log N(HI) < 20.9$ and $\beta = 2.1 \pm 0.9$ for $\log N(HI) \geq 20.9$. The general form of the absolute CDD does not vary considerably with redshift, which in turn explains the roughly constant value of Ω_{DLA} . The differences in the $f(N)$ distributions are subtle, implying that the gas content in DLAs is not changing drastically. This is strong evidence that DLAs do not have high SFRs

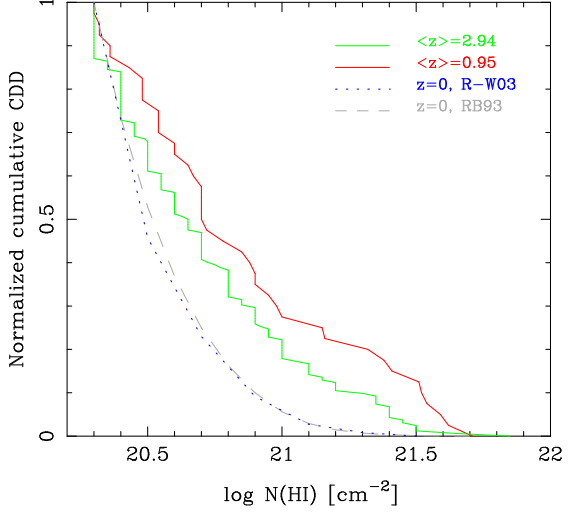


FIG. 17.— The normalized cumulative column density distribution of DLAs for three redshift regimes. The top curve (red, thick solid line) includes the 41 low-redshift DLAs from Table 1 at a median redshift of 0.95. The middle curve (blue, thin solid line) includes 163 high-redshift systems with mean redshift 2.94 (Prochaska & Herbert-Fort 2004), and the bottom two curves are estimates at $z = 0$. The dashed curve is from Rao & Briggs (1993) and the dotted curve is from R-W03.

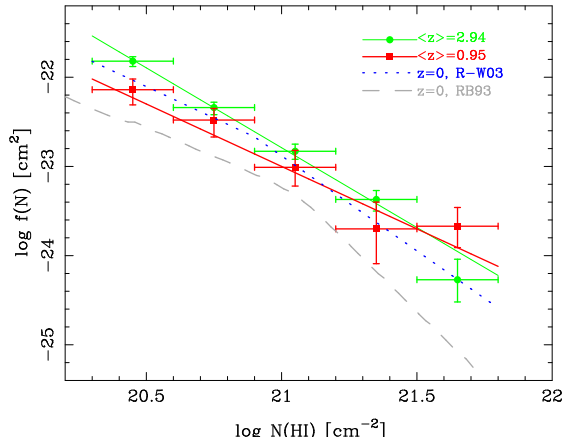


FIG. 18.— Absolute column density distribution (CDD) function for the three redshift regimes. The red, thick solid line is a least squares fit to the low redshift data points and has slope $\beta = 1.4$; the blue, thin solid line is a least squares fit to the high redshift data points with a slope of $\beta = 1.8$. The dotted line is the column density distribution derived by R-W03 from 21 cm HIPASS data of local galaxies. It has slope $\beta = 1.4$ for $\log N(HI) < 20.9$ and $\beta = 2.1$ for $\log N(HI) \geq 20.9$. The dashed line is from HI measurements of an optically-selected sample of local galaxies (Rao & Briggs 1993). The offset between the two $z = 0$ curves arises from the different normalizations of the HI-mass and optical luminosity functions, respectively. See text.

and are, therefore, a different population of objects than those responsible for much of the observed luminosity in the high redshift universe (see also §5.1 and Hopkins et al. 2005). On the other hand, a non-evolving DLA population might be observed if the gas that is used up in star formation is replenished from the inter-galactic medium at a comparable rate. This possibility seems rather contrived, and requires more proof than the current observational evidence can provide. In §5, we discuss further evidence that suggests that DLAs and high SFR galaxies (e.g., Lyman break galaxies) are mutually exclusive

populations.

We'd like to draw the reader's attention to the $z = 0$ curves in Figures 17 and 18. The general shape of the CDD at the present epoch is reproduced in both the RB93 and R-W03 estimates (Figure 17), with only a minor difference in the column density where the slope of the distribution changes (Figure 18). This break in the CDD is a direct consequence of the exponential distribution of $N(HI)$ in disks, with the position of the break depending on the maximum column density in a face-on galaxy. The RB93 CDD was determined using HI 21 cm maps of an optical diameter-limited sample of local galaxies normalized by the luminosity function of late-type galaxies locally (Rao 1994). On the other hand, the R-W03 estimate was derived from the HIPASS survey of HI in the local universe and the HI mass function of galaxies locally (Zwaan et al. 2003). The offset between the two curves (Figure 18) is a result of different normalizations in the luminosity and HI mass functions of the two estimates, respectively. We now know that the local galaxy luminosity function (as determined prior to 1993) did not include gas-rich galaxies that occupy the low-luminosity tail of the galaxy luminosity function. The overall normalization might have been underestimated as well. This offset is also manifested in the values derived for $n(z)$, since $n(z)$ depends on the volume number density of absorbers. In Figure 14, we used the most recent estimate of $n(z = 0) = 0.045 \pm 0.006$ derived by Zwaan et al. (2005a). Ryan-Weber et al. (2005) derive a similar value; these are a factor of 3 higher than the RB93 estimate. It is also of interest to note that the local value of Ω_{HI} derived by RB93 is only $\sim 30\%$ smaller than more recent estimates. This means that while the bulk of the neutral gas at $z = 0$ is in the more luminous galaxies, a significant fraction of the HI cross section is contributed by optically low-surface-brightness and dwarf galaxies. This conclusion is indeed borne out by the recent comparison of HI in low- and high-surface brightness galaxies by Minchin et al. (2004). In any case, it is now clear that the recent deep, large scale surveys of HI gas in the local universe have provided a better understanding of the distribution of HI at $z = 0$, allowing for more precise determinations of its statistical properties for comparison with quasar absorption line studies.

5. DISCUSSION

5.1. Selection Effects and Biases

As with any survey, selection effects and biases need to be well understood in order to correctly interpret results. Here we raise some of the important ones that may affect our survey.

1. We have determined DLA statistics under the assumption that all DLAs exhibit MgII absorption, and therefore, that DLAs form a subset of MgII absorbers. At the redshifts probed by our UV surveys, $0.11 < z < 1.65$, we find that there is little chance of encountering a DLA unless $W_0^{\lambda 2796} \geq 0.6 \text{ \AA}$. Since our MgII sample includes systems with $W_0^{\lambda 2796} \geq 0.3 \text{ \AA}$, we believe this result to be fairly secure. An exception may occur in the rare case where the DLA sightline passes through a single cloud. Its velocity width, i.e., b parameter and therefore, $W_0^{\lambda 2796}$, would then be small, perhaps even smaller than in the DLA towards 3C 286 (see §4.1.1). The DLA

towards the D component of the Cloverleaf gravitationally lensed quasar might be an example of such a case (Monier et al. 2005). The $N(HI) = 2 \times 10^{20} \text{ cm}^{-2}$, $z = 1.49$ DLA is not detected in the three brighter components of this quadruply lensed quasar. A composite Keck spectrum of all four components combined does not detect MgII down to a 3σ limit of $W_0^{\lambda 2796} = 0.06 \text{ \AA}$. Given the relative brightnesses of the four components, any MgII absorption towards component D could be diluted by a factor of 5 - 10 in the composite spectrum. Thus, the absence of metal lines in this DLA need not be an indication of unpolluted gas, but instead, of low velocity dispersion gas that might only be detected with high resolution spectra of component D .

Although the highest redshift DLAs have not been shown to have MgII absorption because the MgII doublet is shifted into the infrared, metals have been detected in DLAs at redshifts as high as $z = 3.9$ (Prochaska et al. 2003a) and are, therefore, expected to also include MgII. Apart from testing the DLA-MgII connection at high redshift and exploring any evolution, assembling a near-infrared MgII sample with follow-up optical spectroscopy to search for DLAs would be important for comparison with blind optical DLA surveys. In addition, Nestor et al. (2003) and Turnshek et al. (2005) have shown that a positive correlation exists between $W_0^{\lambda 2796}$ and neutral gas metallicity when an ensemble average of strong ($W_0^{\lambda 2796} \geq 0.6 \text{ \AA}$) SDSS MgII absorbers is considered. Since the REW of saturated MgII lines is an indication of gas velocity spread, this correlation indicates a metallicity-kinematics relation for the average MgII absorber. The evolution of this relationship to higher redshift will also provide important constraints on CDM simulations of galaxy and structure formation.

Ultimately, our study is based on the premise that all DLAs have MgII absorption, and unless significant counter examples are found, this assumption is now on fairly firm ground.

2. Figure 4 shows that the fraction of DLAs in a MgII sample is a function of $W_0^{\lambda 2796}$, rising from a fraction near 16% just above the threshold value of $W_0^{\lambda 2796} = 0.6 \text{ \AA}$ to about 65% at the highest values near $W_0^{\lambda 2796} = 3 \text{ \AA}$. At present these should be considered approximate fractions since the presence of FeII $\lambda 2600$ has been used to increase the probability of finding a DLA. However, for reasons that are not yet clear, the FeII criterion does not affect the mean HI column density as a function of $W_0^{\lambda 2796}$ (see Figure 7), and so the FeII inclusion effect is probably not significant for our sample. Nevertheless, the $W_0^{\lambda 2796}$ dependence of the DLA fraction will introduce a bias in n_{DLA} unless the observed sample's $W_0^{\lambda 2796}$ distribution matches the true distribution. We have accounted for this by carefully defining our samples as described in §2, and by making use of Equations 1, 2, and 3 to calculate n_{DLA} .

3. The degree to which $N(HI)$ may be biased by $W_0^{\lambda 2796}$ can be seen by examining Figure 5. The mean HI column density of identified DLAs is $N(HI) \approx 2 \times 10^{21} \text{ cm}^{-2}$ when $0.6 \text{ \AA} \leq W_0^{\lambda 2796} < 1.2 \text{ \AA}$, but it seems to decrease by a factor of ≈ 4 at $W_0^{\lambda 2796} \approx 3 \text{ \AA}$. However, inspection of Figure 2 suggests that this trend is not particularly tight nor is it well established for DLAs by themselves. On the other hand, if one considers all the

points in Figure 2, it is clear that the $N(HI)$ distribution changes for different $W_0^{\lambda 2796}$ intervals. It is interesting that in MgII-selected surveys for DLAs, the determination of the cosmological mass density of neutral gas, Ω_{DLA} , has (so far) not revealed any dependency on $W_0^{\lambda 2796}$ selection. This is because in our sample, the increased probability (by a factor of ≈ 4) of finding a DLA at the largest $W_0^{\lambda 2796}$ values is approximately compensated for by the corresponding decrease in mean HI column density (by a factor of ≈ 4) at the largest $W_0^{\lambda 2796}$ values. It is worth pointing out that although the MgII selection criteria lead to reasonably complete samples of DLAs, incompleteness must set in at HI column densities in the sub-DLA regime because systems with $W_0^{\lambda 2796} < 0.3 \text{ \AA}$ can have sub-DLA HI column densities. Therefore, only the $N(HI)$ distribution in the DLA regime can be reliably considered with the available data.

4. Hopkins et al. (2005; see also Rao 2005) have discussed the question of whether the observed population of DLAs can account for the observed SFH of the universe from low to high redshift. By applying the Kennicutt (1998) formulation of the Schmidt law to the properties of the currently observed population of DLAs they find that the DLAs cannot account for the cosmic SFR density inferred from the luminosity density of high-redshift galaxies (see figure 2 in Hopkins et al. 2005). An even larger discrepancy occurs when one compares DLA metallicities to the metallicities expected on the basis of the cosmic SFR (see figure 4 in Hopkins et al. 2005 and figure 13 in Rao 2005). One way to avoid this discrepancy is to postulate that the MgII and blind DLA surveys are not yet large enough to include absorbers with very small individual cross sections that nevertheless may dominate the cosmic SFR and be the main reservoirs for the metals as well. Indeed, these star forming regions will be rich in molecular gas, the direct fuel for star formation, but with HI column densities that may exceed the observed DLA regime. Kennicutt (1998) points out that in normal disks star formation generally takes place in regions that contain $1 - 100 M_{\odot} \text{ pc}^{-2}$ (i.e., $\approx 10^{20} - 10^{22}$ atoms or molecules cm^{-2}), whereas the more rare (and smaller) star burst regions contain $10^2 - 10^5 M_{\odot} \text{ pc}^{-2}$ (i.e., $\approx 10^{22} - 10^{25}$ atoms or molecules cm^{-2}). For example, an absorber with a size of about 100 pc, comparable to giant molecular clouds (GMCs), has a cross section that is $\approx 10^4$ times smaller than known DLAs, which typically have effective radii of $\approx 10 \text{ kpc}$ (Monier et al. 2005). Assuming that there are on the order of 10 GMCs per galaxy, the total cross section per unit volume, i.e., interception probability, for these very high column density gas systems would be on the order of 10^3 times smaller. This means that 10^3 DLAs need to be detected in order to find one very high column density system. With the SDSS, we are getting close, but are not quite there yet. A one in a thousand system with $N(HI + H_2) = 10^{24} \text{ cm}^{-2}$ would increase the SFR density of DLAs by more than a factor of 2, and bring the DLA SFR density into agreement with the luminous SFR density. Searches for molecular gas in DLAs have resulted in only a handful of detections. Moreover, the molecular gas fraction in the few DLAs with H_2 detections is very small (e.g. Ledoux et al. 2003), and is consistent with the idea that the known sample of DLAs

does not trace the majority of the star forming gas in the universe. It therefore seems reasonable to conclude that most of the neutral and molecular gas mass has so far been missed in DLA surveys.

However, the possibility that these very high column density gas systems are being missed by DLA surveys may not only be due to their small gas cross sections, but also because they are likely to be very dusty. Ledoux et al. (2003) find that the DLAs in which H_2 is detected have among the highest metallicities and the highest depletion factors, hinting at the possibility of much higher depletions in much higher column density molecular gas clouds. Although radio loud quasar surveys for DLAs have not revealed any significant dust bias in optical surveys (Ellison et al. 2001; 2004; Akerman et al. 2005), the radio loud quasar surveys for DLAs may themselves suffer from the small cross section selection effect. Not enough radio loud quasars have yet been surveyed to find the putative one in a thousand very high column density system. But if significant mass has been missed due to small total cross section for star forming regions, whether or not these high-gas-mass regions will be found once sample sizes are much larger is unclear. Substantial dust-induced reddening may prevent complete samples from ever being discovered via optical quasar absorption-line spectroscopy.

In this regard it is interesting that Gardner et al. (1997) found in their CDM simulations that depletion of the gas supply by star formation only affected the DLA statistics at $z > 2$ for $N(HI) > 10^{22} \text{ atoms cm}^{-2}$ (i.e., in a regime where DLAs have not been found), even though roughly half of the cold collapsed gas was converted to stars by $z = 2$.

5. Gravitational lensing has the opposite effect on DLA surveys. Magnification by DLA galaxies could brighten background quasars, and preferentially include them in magnitude-limited samples. Le Brun et al. (2000), with HST imaging observations, showed no evidence for multiple images of background quasars and concluded that the quasars were magnified by at most 0.3 magnitudes. In addition, Ellison et al. (2004) and Pérout et al. (2004) using statistical tests on low redshift MgII and DLA samples, showed that lensing bias is a minor effect. More recently, using the SDSS MgII survey results of Nestor (2004), Ménard et al. (2005) show that quasars behind strong MgII absorbers, of which DLAs are a subset, show little magnification bias, and that its effect on Ω_{DLA} at low redshift is negligible (see also Ménard 2005). It is also unlikely that the lowest redshift points that we derived from our HST-UV data (Figure 16) are affected by lensing bias. This is because the DLAs with the highest HI column densities at $z \approx 0.5$ arise in dwarf galaxies (Rao et al. 2003), and consequently, do not have the mass required to produce significant magnification.

5.2. Interpretation of the Statistical Results on DLAs

As discussed in §4, the evolutionary behavior of n_{DLA} , Ω_{DLA} , and the CDD are, at least qualitatively, consistent with one another in terms of a simple galaxy formation scenario. We find evidence for a rapid decline of n_{DLA} (by a factor of 2) from $z = 5$ to $z \approx 2$ followed by no evolution down to $z = 0$. For comparison, the evolution of Ly α forest lines with $\log N(HI) \gtrsim 14$, which

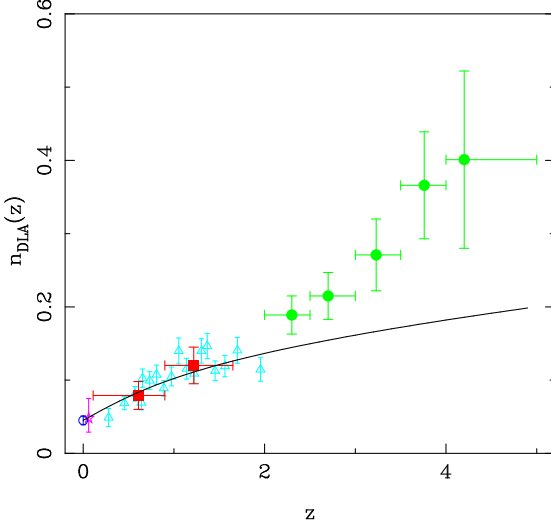


FIG. 19.— Redshift number density of DLAs as a function of redshift. Symbols are the same as in Figure 14 with the addition of open triangles, which are derived from the $W_0^{\lambda 2796} \geq 0.6 \text{ \AA}$ MgII redshift number density and assuming that the fraction of DLAs in these MgII systems is constant at 22%. The errors are therefore indicative of statistical errors in the MgII sample alone. The open star at $z = 0.06$ is similarly derived from the HST MgII sample of Churchill (2001). Including errors in the DLA fraction will systematically move the data up or down by $\sim 25\%$.

have been shown to be associated with the same large scale structure that traces galaxies (Tripp, Lu, & Savage 1998; Davé et al. 1999; Penton, Stocke, & Shull 2002), also slows down dramatically near $z \approx 1.5$ (e.g., Kim et al. 2002, Weymann et al. 1998). Thus, both the DLAs and the higher $N(HI)$ Ly α forest appear to follow similar evolutionary histories consistent with the collapse and assembly of baryonic structures near $z \sim 1.5$ or 2. The near constant value of Ω_{DLA} during the phase of rapid evolution in n_{DLA} implies an increase in the HI column densities of individual clouds. The observed evolution in the CDD of the DLAs, although mild, is evidence for this. The subsequent drop in Ω_{DLA} down to $z = 0$ along with an unevolving n_{DLA} is indicative of star formation that depletes gas while keeping the absorption cross section constant. The change in slope of the CDD from low redshift to $z = 0$, i.e., the decrease in the ratio of high to low column densities, is again consistent with this scenario. Further details on the evolution of HI from low redshift to the present epoch can be studied only when the sample of low-redshift DLAs becomes large enough to split the $0 < z < 1.65$ redshift interval, without compromising on the uncertainties, into finer than the current two bins, and now we consider this possibility by adopting some reasonable assumptions. We have shown that a survey of MgII systems with $W_0^{\lambda 2796} \geq 0.6 \text{ \AA}$ is a reliable tracer of DLAs, and can be used to determine DLA statistics. The two n_{DLA} data points at low redshift shown in Figure 14 are $20 (\pm 5)\%$ and $24 (\pm 6)\%$ of the corresponding MgII redshift number density values for $W_0^{\lambda 2796} \geq 0.6 \text{ \AA}$ derived by Nestor (2004) and NTR05, at $z = 0.6$ and $z = 1.2$ respectively. By assuming that the DLA fraction in a $W_0^{\lambda 2796} \geq 0.6 \text{ \AA}$ sample is constant over the entire redshift interval $0.1 < z < 1.65$, n_{DLA} can be estimated in much smaller redshift bins from the

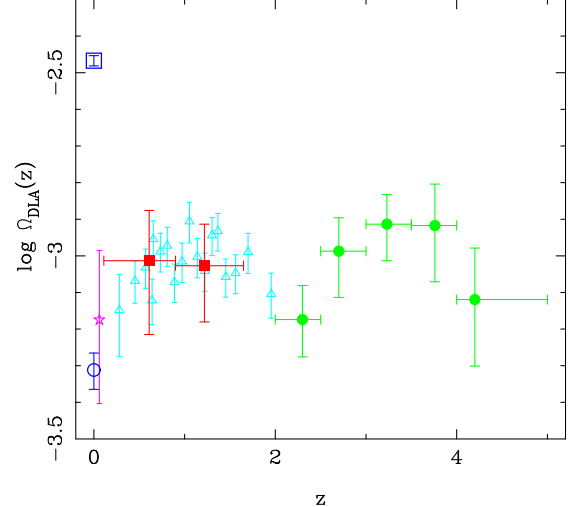


FIG. 20.— Cosmological mass density of neutral gas in DLAs as a function of redshift. Symbols are the same as in Figure 16 with the addition of open triangles, which are derived from the $W_0^{\lambda 2796} \geq 0.6 \text{ \AA}$ MgII redshift number density, and assuming that the fraction of DLAs in these MgII systems is constant at 22% and that their HI column density is constant at $1.16 \times 10^{21} \text{ cm}^{-2}$. The errors are therefore indicative of statistical errors in the MgII sample alone. The open star at $z = 0.06$ is similarly derived from the HST MgII sample of Churchill (2001). Including errors in the DLA fraction and $N(HI)$ will systematically move the data up or down by ~ 0.1 dex. We see, for the first time, possible evidence of a decline in Ω_{DLA} from $z \approx 0.5$ to $z = 0$.

statistics of any MgII survey sample without a UV survey for DLAs. The systematic uncertainty in n_{DLA} will then be primarily limited only by the precision to which the DLA fraction is known. Similarly, the systematic uncertainty in Ω_{DLA} will primarily be limited by how accurately the DLA HI column density is known. For $W_0^{\lambda 2796} \geq 0.6 \text{ \AA}$, we found the mean DLA column density to be $\langle N(HI) \rangle = (1.16 \pm 0.20) \times 10^{21} \text{ cm}^{-2}$. Recall that all the DLAs in our sample have $W_0^{\lambda 2796} \geq 0.6 \text{ \AA}$. Assuming a constant DLA fraction of 22% and a constant DLA HI column density of $1.16 \times 10^{21} \text{ cm}^{-2}$, we can estimate n_{DLA} and Ω_{DLA} from the MgII $W_0^{\lambda 2796} \geq 0.6 \text{ \AA}$ redshift number density as follows (see Equations 1 and 4):

$$n_{DLA}(z) = 0.22 \times n_{MgII}(z) \quad (7)$$

and

$$\Omega_{DLA}(z) = \frac{\mu m_H H_0}{c \rho_c} 0.22 \times n_{MgII}(z) \times 1.16 \times 10^{21} \frac{E(z)}{(1+z)^2}. \quad (8)$$

These data points are shown in Figures 19 and 20 as open triangles. Only the error in n_{MgII} is propagated through to show the statistical uncertainty in these data. The errors associated with the DLA fraction and DLA column density are systematic and will affect all of these data points equally, moving them uniformly up or down by $\sim 25\%$ in the case of n_{DLA} and ~ 0.1 dex for $\log \Omega_{DLA}$. We also show n_{DLA} and Ω_{DLA} inferred using the redshift number density derived by Churchill (2001) for MgII systems detected in HST spectra, $n_{MgII}(z = 0.06) = 0.22^{+0.12}_{-0.09}$; again, only the error in n_{MgII} has been propagated. We now see for the first time that, under the assumption of constant DLA fraction and HI column density suggested by our current MgII-DLA sample, there

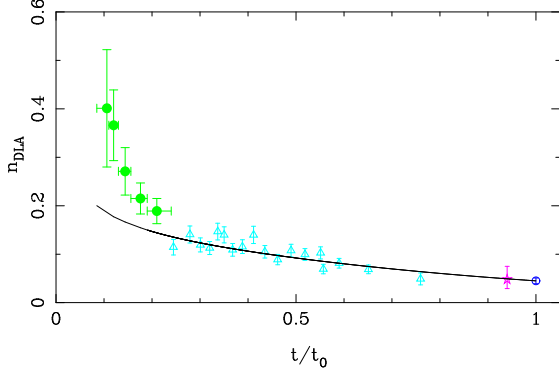


FIG. 21.— Redshift number density of DLAs as a function of cosmic time with t_0 being the current epoch. Symbols are the same as in Figure 19.

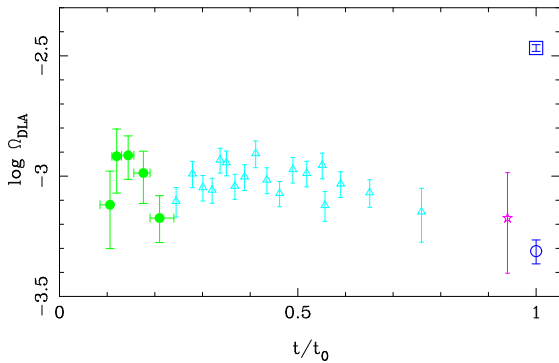


FIG. 22.— Cosmological mass density of neutral gas in DLAs as a function of cosmic time with t_0 being the current epoch. Symbols are the same as in Figure 20.

may be evidence of a decreasing trend in Ω_{DLA} from $z = 0.5$ to $z = 0$. There also appears to be a dip in Ω_{DLA} near $z = 2$, albeit within 1σ , that shows up in both the high- and low-redshift data. It should be noted that the highest of the low redshift data points comes from the red end of SDSS spectra, and suffers from low signal-to-noise ratio due to the presence of atmospheric absorption. Similarly, the lowest of the high redshift data points comes from the blue end of SDSS spectra, and also suffers from low signal-to-noise ratio. Whether this 1σ effect will persist with better quality data remains to be seen; but if real, will be a challenge for galaxy formation models to explain. These two figures illustrate our method for determining DLA statistics. Using our sample of 197 MgII systems with follow-up UV spectra, we have demonstrated that, to first order, the DLA fraction in a $W_0^{\lambda 2796} \geq 0.6$ Å MgII sample and the DLA HI column density are constant. Using this assumption, we have shown that details in the evolution of MgII systems can reveal details in the neutral gas evolution. The data point at $z = 0.28$ was derived from the MMT survey for low redshift MgII systems (Nestor 2004; Nestor, Turnshek, & Rao, in preparation), and is in a redshift regime inaccessible by the SDSS. An even larger survey for MgII systems at $0.11 < z < 0.36$ is clearly needed in order to understand the evolution of Ω_{DLA} in a redshift regime where most of the evolution appears to be taking place. Similarly, a high-redshift, near infrared survey for MgII systems could extend this method into the optical

regime, and any evolution in the MgII-DLA relationship could be studied. In order to underscore the importance of pursuing this work in the future, we show n_{DLA} and Ω_{DLA} as functions of cosmic time in Figures 21 and 22, respectively.

6. SUMMARY

We have presented statistical results on UV surveys for low-redshift ($z < 1.65$) DLAs with $N(HI) \geq 2 \times 10^{20}$ cm $^{-2}$ using the largest sample of UV-detected DLAs ever assembled. The DLAs were found by targeting QSOs with MgII systems identified optically in the redshift range $0.11 < z < 1.65$. In total, UV observations of the Ly α absorption line in 197 MgII systems with $W_0^{\lambda 2796} \geq 0.3$ Å have been obtained. This is an efficient and effective way to find DLAs because, in the absence of MgII, the system evidently has no chance of being a DLA. This sample contains 41 DLAs, all of which have $W_0^{\lambda 2796} \geq 0.6$ Å. Our main findings can be summarized as follows:

1. To a high level of completeness, DLAs can be studied through follow-up observations of strong MgII absorbers. In particular, Figure 4 shows that for our sample the probability of a MgII system being a DLA is $P \approx 0$ for $W_0^{\lambda 2796} < 0.6$ Å and $P \approx 0.16 + 0.18(W_0^{\lambda 2796} - 0.6)$ for $0.6 \leq W_0^{\lambda 2796} < 3.3$ Å. A MgII absorber must generally have $1 < W_0^{\lambda 2796}/W_0^{\lambda 2600} < 2$ and $W_0^{\lambda 2852} > 0.1$ Å to be a DLA (see §4.1).

2. UV spectroscopy, almost exclusively with HST, enabled us to measure or place limits on $N(HI)$ for each of the 197 systems studied. For MgII systems with $0.3 \text{ \AA} \leq W_0^{\lambda 2796} < 0.6 \text{ \AA}$, $\langle N(HI) \rangle = (9.7 \pm 2.2) \times 10^{18}$ cm $^{-2}$, while for systems with $W_0^{\lambda 2796} \geq 0.6 \text{ \AA}$, $\langle N(HI) \rangle = (3.5 \pm 0.7) \times 10^{20}$ cm $^{-2}$. This is basically a step function (see Figure 4), with a factor of ≈ 36 change in mean HI column density near $W_0^{\lambda 2796} \approx 0.6$ Å. Since the MgII absorption lines are saturated at $W_0^{\lambda 2796} > 0.6$ Å, there is evidently a threshold in kinematic velocity spread below which it is highly unlikely to encounter high column density neutral DLA gas.

3. Above $W_0^{\lambda 2796} = 0.6$ Å, the mean HI column density of a sample of MgII absorbers is found to be constant with increasing $W_0^{\lambda 2796}$. However, owing to the increase in probability of finding a DLA with increasing $W_0^{\lambda 2796}$, the mean HI column density of MgII absorbers that are DLAs is found to decrease by about a factor of four with increasing $W_0^{\lambda 2796}$, from $W_0^{\lambda 2796} \approx 0.6$ Å to $W_0^{\lambda 2796} \approx 3.5$ Å. Improved statistics are needed to study this effect owing to the large scatter in the $W_0^{\lambda 2796}$ versus $N(HI)$ plane for $W_0^{\lambda 2796} > 0.6$ Å.

4. By combining results at all redshifts, including 21 cm emission surveys at $z = 0$, we find that the DLA incidence per unit redshift can be parameterized as $n_{DLA}(z) = n_0(1 + z)^\gamma$ where $n_0 = 0.044 \pm 0.005$ and $\gamma = 1.27 \pm 0.11$. In the standard “737” cosmology this indicates no evolution in the product of neutral gas cross section times comoving number density at redshifts $z \lesssim 2$, but from $z \approx 5$ to $z \approx 2$ there is a decrease of a factor of ≈ 2 in this quantity relative to the no evolution prediction (Figure 19). This decline happens relatively rapidly, in a time span that corresponds to $\lesssim 1.5$ Gyrs.

5. The cosmological mass density of neutral gas due to DLAs, Ω_{DLA} , follows a completely different evolutionary pattern. It remains relatively constant in the redshift in-

terval $0.5 < z < 5.0$, with $\Omega_{DLA} \approx 10^{-3}$, but then it declines by a factor of ≈ 2 between $z \approx 0.5$ and $z = 0$ (Figure 20). This drop in neutral gas takes place during the last ≈ 5 Gyrs of the history of the Universe. However, due to possible selection effects which are biased against finding regions with very high column densities because the product of their gas cross section and comoving number density is small, it is important to realize that the neutral gas component as traced by the DLAs may not include all of the neutral and molecular gas involved in star formation (Hopkins et al. 2005; Rao 2005; Turnshek et al. 2005).

6. Consistent with the $n_{DLA}(z)$ and $\Omega_{DLA}(z)$ results, the HI CDD at $\langle z \rangle \approx 1$ shows a higher incidence of high column density systems than at $\langle z \rangle \approx 3$. This presumably represents a build up of neutral mass concentrations. By $z = 0$ the higher incidence of high $N(HI)$ systems seen at $\langle z \rangle \approx 1$ has disappeared, presumably due to the depletion of gas during star formation.

7. In the absence of future QSO absorption-line surveys that aim to identify DLAs and measure their $N(HI)$ in UV spectra, more detailed studies that lead to a better understanding of the strong MgII systems may hold promise for reaching a better determination of the prop-

erties of the neutral gas phase of the universe at $z < 1.65$ (e.g., Figures 19 – 22).

This work was funded by grants from NASA-STScI, NASA-LTSA, and NSF. HST-UV spectroscopy made the $N(HI)$ determinations possible. We thank members of the SDSS collaboration who made the SDSS project a success. Funding for creation and distribution of the SDSS Archive has been provided by the Alfred P. Sloan Foundation, Participating Institutions, NASA, NSF, DOE, the Japanese Monbukagakusho, and the Max Planck Society. The SDSS Web site is www.sdss.org. The SDSS is managed by the Astrophysical Research Consortium for the Participating Institutions: University of Chicago, Fermilab, Institute for Advanced Study, the Japan Participation Group, Johns Hopkins University, Los Alamos National Laboratory, the Max-Planck-Institute for Astronomy (MPIA), the Max-Planck-Institute for Astrophysics (MPA), New Mexico State University, University of Pittsburgh, Princeton University, the United States Naval Observatory, and University of Washington.

REFERENCES

Akerman, C. J., Ellison, S. L., Pettini, M., & Steidel, C. C. 2005, *A&A*, in press (astro-ph/0506180)

Akritas, M. G., & Bershady, M. A. 1996, *ApJ*, 470, 706

Aldcroft, T. L., Bechtold, J., & Elvis, M. 1994, *ApJS*, 93, 1

Bahcall, J. et al. 1993, *ApJS*, 87, 1

Barthel, P. D., Tytler, D. R., & Thomson, B. 1990, *A&AS*, 82, 339

Bergeron, J. & Boissé, P. 1984, *A&A*, 133, 374

Bergeron, J. & D'Odorico, S. 1986, *MNRAS*, 220, 833

Bergeron, J., & Stasińska, G. 1986, *A&A*, 169, 1

Bergeron, J., D'Odorico, S., & Kunth, D. 1987, *A&A*, 180, 1

Bergeron, J., & Boisse, P. 1991, *A&A*, 243, 344

Boissé, P., & Bergeron, J. 1985, *A&A*, 145, 59

Boissé, P., Boulade, O., Kunth, D., Tytler, D. & Vigroux, L. 1992, *A&A*, 262, 401

Boksenberg, A., Carswell, R. F., & Sargent, W. L. W. 1979, *ApJ*, 227, 370

Briggs, F. H. & Wolfe, A. M. 1983, *ApJ*, 268, 76

Caulet, A. 1989, *ApJ*, 340, 90

Calura, F. & Matteucci, F. 2004, *MNRAS*, 350, 351

Cen, R., & Ostriker, J. 1999, *ApJ*, 514, 1

Churchill, C. W. 2001, *ApJ*, 560, 92

Churchill et al. 2000, *ApJS*, 130, 91

Churchill, C. W., Vogt, S. S., & Charlton, J. C. 2003, *AJ*, 125, 98

Cohen, R. D., Barlow, T. A., Beaver, E. A., Junkkarinen, V. T., Lyons, R. W., & Smith, H. E. 1994, *ApJ*, 421, 453

Curran, S. J., Murphy, M. T., Pihlström, Y. M., Webb, J. K., & Purcell, C. R. 2005, *MNRAS*, 356, 1509

Davé, R., Hernquist, L., Katz, N., & Weinberg, D. 1999, *ApJ*, 511, 521

Dinshaw, N., & Impey, C. 1996, *ApJ*, 458, 73

Ellison, S. L., Yan, L., Hook, I. M., Pettini, M., Wall, J., & Shaver, P. 2001, *A&A*, 379, 393

Ellison, S. L., Churchill, C. W., Rix, S. A., & Pettini, M. 2004, *ApJ*, 615, 118

Falomo, R. 1990, *ApJ*, 353, 114

Foltz, C. B., Weymann, R. J., Peterson, B. M., Sun, L., Malkan, M. A., & Caffee Jr., F. H. 1986, *ApJ*, 307, 504

Fukugita, M., & Peebles, P. J. E. 2004, *ApJ*, 616, 643

Haehnelt, M. G., Steinmetz, M., & Rauch, M. 1998, *ApJ*, 495, 647

Hopkins, A. M., Rao, S. M., & Turnshek, D. A. 2005, *ApJ*, 630, 108

Jannuzzi, B. T. et al. 1998, *ApJS*, 118, 1

Kanekar, N. & Chengalur, J. 2001, *MNRAS*, 325, 631

Kanekar, N. & Chengalur, J. 2003, *A&A*, 399, 857

Kanekar, N., Ghosh, T., & Chengalur, J. N. 2001, *A&A*, 373, 394

Kennicutt, R. C. 1998, *ApJ*, 498, 541

Kim, T.-S., Carswell, R. F., Cristiani, S., D'Odorico, S., & Giallongo, E. 2002, *MNRAS*, 335, 555

Khare, P. et al. 2004, *ApJ*, 616, 86

Kunth, D. & Bergeron, J. 1984, *MNRAS*, 210, 873

Lane, W. 2000, Ph.D. Thesis, Univ. Groningen

Lane, W. M. & Briggs, F. H. 2001, in *ASP Conf. Ser.* 254, *Extragalactic Gas at Low Redshift*, ed. J. Mulchaey & J. Stocke (San Francisco: ASP), 189

Lane, W. M., Briggs, F. H., Smette, A. 2000, *ApJ*, 532, 146

Lanzetta, K. M., Wolfe, A. M., Turnshek, D. A., Lu, L., McMahon, R. G., & Hazard, C. 1991, *ApJS*, 77, 1

Lanzetta, K. M., Turnshek, D. A., & Wolfe, A. M. 1987, *ApJ*, 322, 739

Lanzetta, K. M., Wolfe, A. M., & Turnshek, D. A. 1995, *ApJ*, 440, 435

Le Brun, V., Bergeron, J., Boissé, P., & Christian, C. 1993, *A&A*, 279, 33

Le Brun, V., Bergeron, J., Boissé, P., & Deharveng, J. M. 1997, *A&A*, 321, 733

Le Brun, V., Smette, A., Surdej, J., & Claejkens, J.-F. 2000, *A&A*, 363, 837

Ledoux, C., Petitjean, P., & Srianand, R. 2003, *MNRAS*, 346, 209

Lu, L., Wolfe, A. M., Turnshek, D. A., & Lanzetta, K. M. 1993, *ApJS*, 84, 1

Lu, L., & Wolfe, A. M. 1994, *AJ*, 108, 44

Ménard, B. 2005, *ApJ*, 630, 28

Ménard, B., et al. 2005, in preparation

Miller, J. S. & French, H. B. 1978, *Pitts. Conf. on BL Lac Objects*, ed. A. M. Wolfe (U. Pittsburgh), 228

Minchin, R. F., et al. 2004, *MNRAS*, 355, 1303

Monier, E. M., Turnshek, D. A., & Rao, S. M. 2005, in preparation

Nestor, D. B. 2004, Ph.D. Thesis, Univ. Pittsburgh

Nestor, D. B., Rao, S., Turnshek, D. A., & Vanden Berk, D. 2003, *ApJ*, 595, L5

Nestor, D. B., Turnshek, D. A., & Rao, S. 2005, *ApJ*, 628, 637 (NTR05)

Panter, B., Heavens, A. F., & Jimenez, R. 2004, *MNRAS*, 355, 764

Penton, S. V., Stocke, J. T., & Shull, J. M. 2002, *ApJ*, 565, 720

Péroux, C., McMahon, R. G., Storrie-Lombardi, L. J., & Irwin, M. J. 2003, *MNRAS*, 346, 1103

Péroux, C., Deharveng J.-M., Le Brun, V., & Cristiani, S. 2004, *MNRAS*, 352, 1291

Péroux, C., Dessauges-Zavadsky, M., D'Odorico, S., Kim, T. S., & McMahon, R. G. 2005, *MNRAS*, submitted

Petitjean, P., & Bergeron, J. 1990, *A&A*, 231, 309

Prochaska, J. X. & Wolfe, A. M. 1997, *ApJ*, 487, 73

Prochaska, J. X. & Wolfe, A. M. 1998, *ApJ*, 507, 113

Prochaska, J. X., Gawiser, E., Wolfe, A. M., Cooke, J., & Gelino, D. 2003a, *ApJS*, 147, 227

Prochaska, J. X., Gawiser, E., Wolfe, A. M., Castro, S., & Djorgovski, S. G. 2003b, *ApJ*, 595, L9

Prochaska, J. X. & Herbert-Fort, S. 2004, *PASP*, 116, 622

Rao, S. M. 1994, Ph.D. Thesis, Univ. Pittsburgh

Rao, S. M. 2005, in *Probing Galaxies through Quasar Absorption Lines*, IAU 199, P. Williams, C. Shu, and B. Ménard eds.

Rao, S. M. & Briggs, F. H. 1993, *ApJ*, 419, 515

Rao, S. M., Turnshek, D. A., & Briggs, F. H. 1995, *ApJ*, 449, 488 (RTB95)

Rao, S. M. & Turnshek, D. A. 1998, *ApJ*, 500, L115

Rao, S. M. & Turnshek, D. A. 2000, *ApJS*, 130, 1 (RT00)

Rao, S. M., Nestor, D. B., Turnshek, D. A., Lane, W. M., Monier, E. M., & Bergeron, J. 2003, *ApJ*, 595, 94

Rao, S. M. & Turnshek, D. A. 2000, *ApJS*, 130, 1 (RT00)

Rao, S. M., Prochaska, J. X., Howk, J. C., & Wolfe, A. M. 2005, *AJ*, 129, 9

Ryan-Weber, E. V., Webster, R. L., Staveley-Smith, L. 2003, *MNRAS*, 343, 1195 (R-W03)

Ryan-Weber, E. V., Webster, R. L., Staveley-Smith, L. 2005, *MNRAS*, 356, 1600

Sargent, W. L. W., Young, P. J., & Boksenberg, A. 1982, *ApJ*, 252, 54

Sargent, W. L. W., Boksenberg, A., & Steidel, C. C. 1988, *ApJS*, 68, 539

Sargent, W. L. W., Steidel, C. C., & Boksenberg, A. 1989, *ApJS*, 69, 703

Steidel, C. C., 1990, *ApJS*, 72, 1

Steidel, C. C. & Sargent, W. L. W. 1992, *ApJS*, 80, 1 (SS92)

Storrie-Lombardi, L. J., & Wolfe, A. M. 2000, *ApJ*, 543, 552

Tripp, T. M., Lu, L., & Savage, B. D. 1998, *ApJ*, 508, 200

Turnshek, D. A., Wolfe, A. M., Lanzetta, K. M., Briggs, F. H., Cohen, R. D., Foltz, C. B., Smith, H. E., & Wilkes, B. J. 1989, *ApJ*, 344, 567

Turnshek, D. A., Rao, S. M., Nestor, D. B., Lane, W. M., Monier, E. M., Bergeron, J., & Smette, A. 2001, *ApJ*, 553, 288

Turnshek, D. A., Rao, S. M., Nestor, Vanden Berk, D., Belfort-Mihalyi, M., & Monier, E. M. 2004, *ApJ*, 609, L53

Turnshek, D. A., Rao, S. M., Nestor, D. B., Belfort-Mihalyi, M., & Quider, A. 2005, in *Probing Galaxies through Quasar Absorption Lines*, IAU 199, P. Williams, C. Shu, and B. Ménard eds.

Tytler, D., Boksenberg, A., Sargent, W. L. W., Young, P., & Kunth, D. 1987, *ApJS*, 64, 667

Ulrich, M.-H., & Owen, F. N. 1977, *Nature*, 269, 673

Weymann, R. J., et al. 1998, *ApJ*, 506, 1

Wills, B. J. 1978, Pitts. Conf. on BL Lac Objects, ed. A. M. Wolfe (U. Pittsburgh), 235

Wills, B. J., & Wills, D. 1980, *ApJ*, 238, 1

Wolfe, A. M., Turnshek, D. A., Smith, H. E., & Cohen, R. D. 1986, *ApJS*, 61, 249

Wolfe, A. M., Turnshek, D. A., Lanzetta, K. M., & Lu, L. 1993, *ApJ*, 404, 480

Wolfe, A. M., Prochaska, J. X., & Gawiser, E. 2003, *ApJ*, 593, 215

Wright, A. E., Morton, D. C., Peterson, B. A., & Jauncey, D. L. 1982, *MNRAS*, 199, 81

Young, D., Sargent, W. L. W., & Boksenberg, A. 1982, *ApJS*, 48, 455

Zwaan, M. A., et al. 2003, *AJ*, 125, 2842

Zwaan, M. A., van der Hulst, J. M., Briggs, F. H., Verheijen, M. A. W., & Ryan-Weber, E. V. 2005a, *astro-ph/0508232*

Zwaan, M. A., Meyer, M. J., Staveley-Smith, L., Webster, R. L. 2005b, *MNRAS*, 359, 30

TABLE 1
 THE MG II SAMPLE^a

QSO	<i>m</i> _V	<i>z</i> _{em}	<i>z</i> _{abs} MgII	<i>W</i> ₀ ^{λ2600} (Å) FeII	<i>W</i> ₀ ^{λ2796} (Å) MgII	<i>W</i> ₀ ^{λ2803} (Å) MgII	<i>W</i> ₀ ^{λ2852} (Å) MgI	Refs	log N(HI) ^b	Sel ^c	UV sp ^d
									Crit	source	
0002-422	17.2	2.758	1.5413	<0.1	0.48 ± 0.04	0.32 ± 0.04	0.27 ± 0.06	1	18.86 ^{+0.02} -0.02	1	06
0002+051	16.2	1.899	0.8514	0.42 ± 0.02	1.09 ± 0.02	0.84 ± 0.03	0.17 ± 0.03	2	19.08 ^{+0.03} -0.04	1	AR
0009-016	17.6	1.998	1.3862	0.46 ± 0.04	0.88 ± 0.08	0.74 ± 0.09	...	2	20.26 ^{+0.02} -0.02	2	09
0017+154	18.2	2.018	1.6261	0.83	1.42	1.30	...	3	19.41 ^{+0.05} -0.05	3	09
0021+0043	17.7	1.245	0.5203	0.280 ± 0.072	0.533 ± 0.036	0.342 ± 0.033	0.048 ± 0.040	4	19.54 ^{+0.02} -0.03	1	11
...	0.9420	0.942 ± 0.036	1.777 ± 0.035	1.735 ± 0.037	0.576 ± 0.044	4	19.38 ^{+0.10} -0.15	4	11
0021+0104	18.2	1.829	1.3259	2.251 ± 0.090	2.656 ± 0.076	2.414 ± 0.071	0.535 ± 0.069	4	20.04 ^{+0.07} -0.14	4	11
...	1.5756	1.802 ± 0.060	3.264 ± 0.084	2.595 ± 0.080	...	4	20.48 ^{+0.12} -0.18	4	11
0041-266	17.8	3.053	0.8626	...	0.67 ± 0.06	0.38 ± 0.06	<0.1	5	< 18.00	2	09
0058+019	17.2	1.959	0.6127	1.27 ± 0.04	1.63 ± 0.01	1.51 ± 0.03	0.30 ± 0.06	6,7	20.04 ^{+0.10} -0.09	1	06
0106+0105	19.0	1.611	1.3002	1.181 ± 0.122	2.050 ± 0.088	1.747 ± 0.074	0.429 ± 0.110	4	20.95 ^{+0.05} -0.11	4	11
...	1.3556	0.164 ± 0.118	1.312 ± 0.094	0.716 ± 0.079	-0.066 ± 0.100	4	19.65 ^{+0.09} -0.11	1	11
0107-0019	18.3	0.738	0.5260	...	0.784 ± 0.080	0.488 ± 0.065	-0.073 ± 0.065	4	18.48 ^{+0.30} -0.63	1	11
0116-0043	18.7	1.282	0.9127	0.904 ± 0.104	1.379 ± 0.096	1.115 ± 0.095	-0.001 ± 0.114	4	19.95 ^{+0.05} -0.11	4	11
0117+213	16.1	1.491	0.5764	0.88 ± 0.04	0.91 ± 0.04	0.93 ± 0.04	0.23 ± 0.04	2	19.15 ^{+0.06} -0.07	1	AR
...	1.0480	0.07 ± 0.01	0.42 ± 0.01	0.26 ± 0.03	0.03 ± 0.01	2,7	18.86 ^{+0.02} -0.02	1	AR
0119-046	16.9	1.953	0.6577	<0.1	0.30 ± 0.04	0.22 ± 0.04	<0.1	8	18.76 ^{+0.09} -0.07	1	06
0123-0058	18.6	1.551	0.8686	0.231 ± 0.071	0.757 ± 0.098	0.746 ± 0.116	0.077 ± 0.093	4	< 18.62	1	11
...	1.4094	1.503 ± 0.062	1.894 ± 0.054	1.795 ± 0.054	0.610 ± 0.073	4	20.08 ^{+0.10} -0.08	4	11
0126-0105	18.4	1.609	1.1916	1.374 ± 0.072	1.983 ± 0.055	1.798 ± 0.060	0.518 ± 0.061	4	20.60 ^{+0.02} -0.06	4	11
0132+0116	18.9	1.786	1.2712	1.848 ± 0.144	2.739 ± 0.108	2.509 ± 0.144	0.931 ± 0.115	4	19.70 ^{+0.08} -0.10	4	11
0138-0005	18.7	1.340	0.7821	1.103 ± 0.110	1.208 ± 0.096	1.384 ± 0.102	0.278 ± 0.094	4	19.81 ^{+0.06} -0.11	4	11
0139-0023	19.0	1.384	0.6828	1.067 ± 0.098	1.243 ± 0.102	1.123 ± 0.121	0.592 ± 0.117	4	20.60 ^{+0.05} -0.12	4	11
0141+339	17.6	1.450	0.4709	<0.7	0.78 ± 0.07	0.65 ± 0.07	<0.3	2	18.88 ^{+0.08} -0.10	1	06
0143-015	17.7	3.141	1.0383	<0.1	0.64 ± 0.06	0.53 ± 0.05	<0.1	9	19.15 ^{+0.06} -0.10	1	06
...	1.2853	<0.1	0.56 ± 0.05	0.33 ± 0.04	<0.1	9	18.83 ^{+0.03} -0.03	1	06
0150-202	17.4	2.147	0.7800	<0.3	0.36 ± 0.04	0.21 ± 0.04	...	6	18.87 ^{+0.11} -0.14	1	06
0152+0023	17.7	0.589	0.4818	0.884 ± 0.061	1.340 ± 0.057	0.949 ± 0.050	0.624 ± 0.067	4	19.78 ^{+0.07} -0.08	4	11
0153+0009	17.8	0.837	0.7714	1.217 ± 0.061	2.960 ± 0.051	2.431 ± 0.058	0.755 ± 0.066	4	19.70 ^{+0.08} -0.10	4	11
0153+0052	19.0	1.162	1.0599	1.219 ± 0.078	1.618 ± 0.096	1.375 ± 0.117	0.305 ± 0.126	4	20.43 ^{+0.10} -0.11	4	11
0157-0048	17.9	1.548	1.4157	0.812 ± 0.050	1.292 ± 0.050	1.068 ± 0.044	0.445 ± 0.058	4	19.90 ^{+0.07} -0.06	4	11
0215+015	16.0	1.715	1.3447	1.36 ± 0.02	1.93 ± 0.02	1.64 ± 0.02	0.32 ± 0.02	10	19.89 ^{+0.08} -0.09	1	AR
0239-154	18.4	2.786	1.3035	<0.1	1.04 ± 0.07	0.89 ± 0.07	...	9	< 18.70	2	09
0248+430	17.6	1.310	0.3939	1.03 ± 0.09	1.86 ± 0.09	1.42 ± 0.09	0.70 ± 0.08	2	21.59 ^{+0.06} -0.07	1	06
...	0.4515	<0.1	0.34 ± 0.07	0.29 ± 0.07	<0.5	11	< 19.51	1	06
0253+0107	18.8	1.035	0.6317	2.205 ± 0.182	2.571 ± 0.166	2.581 ± 0.161	1.326 ± 0.157	4	20.78 ^{+0.12} -0.08	4	11
0254-334	16.0	1.849	0.2125	...	2.23	1.73	...	12	19.41 ^{+0.09} -0.14	2	09
0256+0110	18.8	1.349	0.7254	2.467 ± 0.094	3.104 ± 0.115	2.861 ± 0.116	1.021 ± 0.146	4	20.70 ^{+0.11} -0.22	4	11
0302-223	16.4	1.409	1.0096	0.63 ± 0.02	1.16 ± 0.04	0.96 ± 0.04	0.18 ± 0.03	13	20.36 ^{+0.04} -0.04	1	AR
0316-203	19.5	2.869	1.4026	<0.1	0.92 ± 0.06	0.52 ± 0.05	...	9	18.68 ^{+0.14} -0.22	2	09
0333+321	17.5	1.259	0.9531	<0.2	0.47 ± 0.05	0.33 ± 0.04	<0.3	2	< 18.00	1	AR
0352-275	17.9	2.823	1.4051	1.68 ± 0.04	2.75 ± 0.07	2.54 ± 0.07	...	9	20.18 ^{+0.12} -0.18	3	09
0420-014	17.0	0.915	0.6331	...	1.02 ± 0.10	0.86 ± 0.10	...	14	18.54 ^{+0.07} -0.10	2	09

TABLE 1 — *Continued*

QSO	m_V	z_{em}	z_{abs} MgII	$W_0^{\lambda 2600}$ (Å) FeII	$W_0^{\lambda 2796}$ (Å) MgII	$W_0^{\lambda 2803}$ (Å) MgII	$W_0^{\lambda 2852}$ (Å) MgI	Refs	$\log N(\text{HI})^b$	Sel ^c Crit	UV sp ^d source
0421+019	17.0	2.055	1.3918	<0.1	0.34 ± 0.07	0.31 ± 0.07	<0.3	2	< 18.48	1	06
...	1.6379	<0.4	0.34 ± 0.04	0.28 ± 0.05	<0.2	2	$18.88^{+0.03}_{-0.04}$	1	06
0424-131	17.5	2.166	1.4080	0.44 ± 0.05	0.55 ± 0.07	0.35 ± 0.07	<0.3	2	$19.04^{+0.04}_{-0.04}$	1	06
...	1.5623	<0.2	0.38 ± 0.05	0.39 ± 0.05	<0.2	2	$18.90^{+0.04}_{-0.04}$	1	06
0449-168	18.0	2.679	1.0072	1.88 ± 0.05	2.14 ± 0.06	2.13 ± 0.07	0.43 ± 0.05	6	$20.98^{+0.06}_{-0.07}$	3	09
0454+039	16.5	1.343	0.8596	1.23 ± 0.01	1.45 ± 0.01	1.40 ± 0.06	0.31 ± 0.02	2,7	$20.67^{+0.03}_{-0.03}$	1	AR
...	1.1532	0.08 ± 0.02	0.43 ± 0.01	0.36 ± 0.04	0.03 ± 0.01	2,7	$18.59^{+0.03}_{-0.02}$	1	AR
0454-220	16.1	0.534	0.4744	0.98 ± 0.03	1.38 ± 0.01	1.31 ± 0.04	0.33 ± 0.01	15,7	$19.45^{+0.02}_{-0.03}$	1	AR
...	0.4833	0.16 ± 0.04	0.43 ± 0.01	0.27 ± 0.03	0.07 ± 0.01	15	$18.65^{+0.02}_{-0.02}$	1	AR
0710+119	16.6	0.768	0.4629	<0.4	0.62 ± 0.06	0.29 ± 0.05	0.24 ± 0.08	14	< 18.30	1	AR
0729+818	17.5	1.024	0.7068	0.52 ± 0.04	1.27 ± 0.14	0.97 ± 0.14	...	2	$18.67^{+0.06}_{-0.07}$	3	09
0735+178	14.9	...	0.4240	0.87 ± 0.18	1.32 ± 0.03	1.03 ± 0.03	0.18 ± 0.03	16	< 19.00	1	AR
0738+313	16.1	0.630	0.2213	<0.6	0.61 ± 0.04	0.38 ± 0.02	0.24 ± 0.04	17	$20.90^{+0.07}_{-0.08}$	1	06
0742+318	15.6	0.462	0.1920	...	0.33 ± 0.04	0.23 ± 0.04	<0.2	18	< 18.30	1	AR
0823-223	16.2	0.000	0.9110	0.42 ± 0.03	1.28 ± 0.02	0.68 ± 0.10	0.22 ± 0.03	19,7	$19.04^{+0.04}_{-0.04}$	1	06
0827+243	17.3	0.941	0.5247	1.90	2.90	2.20	...	20,21	$20.30^{+0.04}_{-0.05}$	1	06
0843+136	17.8	1.877	0.6064	<0.7	1.08 ± 0.08	0.67 ± 0.09	<0.1	22	$19.56^{+0.11}_{-0.14}$	1	06
0933+732	17.3	2.525	1.4789	0.76 ± 0.08	0.95 ± 0.08	1.15 ± 0.08	<0.3	2	$21.62^{+0.08}_{-0.09}$	1	06
...	1.4973	1.15 ± 0.09	1.71 ± 0.09	1.98 ± 0.09	0.67 ± 0.06	2	$20.00^{+0.18}_{-0.30}$	1	06
0952+179	17.2	1.478	0.2377	...	0.63 ± 0.11	0.79 ± 0.11	<0.4	2	$21.32^{+0.05}_{-0.06}$	1	06
0953-0038	18.4	1.383	0.6381	1.029 ± 0.139	1.668 ± 0.080	1.195 ± 0.083	0.143 ± 0.135	4	$19.90^{+0.07}_{-0.09}$	4	11
0957+003	17.6	0.907	0.6720	...	1.77	1.32	...	23	$19.59^{+0.03}_{-0.03}$	2	09
0957+561A	17.0	1.414	1.3911	1.67 ± 0.21	2.12 ± 0.03	1.97 ± 0.03	0.19 ± 0.04	24,25	$20.32^{+0.09}_{-0.12}$	1	AR
0958+551	16.0	1.760	0.2413	...	0.55 ± 0.07	0.38 ± 0.07	<0.2	6	$19.80^{+0.08}_{-0.09}$	1	06
0959-0035	18.9	1.871	1.5985	1.548 ± 0.064	2.310 ± 0.092	1.770 ± 0.104	0.188 ± 0.076	4	$20.54^{+0.10}_{-0.10}$	4	11
1007+0042	19.1	1.681	0.9321	0.127 ± 0.113	0.896 ± 0.148	0.528 ± 0.143	-0.360 ± 0.146	4	$18.60^{+0.26}_{-0.26}$	1	11
...	1.0373	1.990 ± 0.184	2.980 ± 0.233	3.275 ± 0.260	0.648 ± 0.255	4	$21.15^{+0.15}_{-0.24}$	4	11
1009-0026	17.4	1.244	0.8426	0.403 ± 0.043	0.713 ± 0.038	0.629 ± 0.038	0.135 ± 0.044	4	$20.20^{+0.05}_{-0.06}$	1	11
...	0.8866	1.068 ± 0.039	1.900 ± 0.039	1.525 ± 0.039	0.326 ± 0.046	4	$19.48^{+0.01}_{-0.08}$	4	11
1009+0036	19.0	1.699	0.9714	1.081 ± 0.078	1.093 ± 0.111	1.361 ± 0.131	0.226 ± 0.129	4	$20.00^{+0.11}_{-0.06}$	4	11
1010+0003	18.2	1.399	1.2651	0.973 ± 0.110	1.122 ± 0.069	1.118 ± 0.058	0.420 ± 0.068	4	$21.52^{+0.06}_{-0.07}$	4	11
1010-0047	18.0	1.671	1.0719	0.172 ± 0.109	0.571 ± 0.083	0.449 ± 0.078	-0.034 ± 0.077	4	$18.90^{+0.03}_{-0.03}$	1	11
...	1.3270	1.339 ± 0.060	2.059 ± 0.051	1.859 ± 0.047	0.298 ± 0.048	4	$19.81^{+0.03}_{-0.07}$	4	11
1019+309	17.5	1.319	0.3461	...	0.70 ± 0.05	0.68 ± 0.05	...	2	$18.18^{+0.08}_{-0.10}$	2	09
1022+0101	18.9	1.563	1.4240	0.414 ± 0.146	0.862 ± 0.074	0.383 ± 0.070	0.095 ± 0.088	4	$18.97^{+0.07}_{-0.03}$	1	11
1028-0100	18.2	1.531	0.6322	1.140 ± 0.101	1.579 ± 0.087	1.216 ± 0.093	0.568 ± 0.091	4	$19.95^{+0.05}_{-0.08}$	4	11
...	0.7087	0.888 ± 0.091	1.210 ± 0.066	1.008 ± 0.068	0.718 ± 0.088	4	$20.04^{+0.07}_{-0.04}$	4	11
1032+0003	18.9	1.193	1.0168	0.697 ± 0.119	1.919 ± 0.128	1.650 ± 0.130	-0.083 ± 0.160	4	$19.00^{+0.04}_{-0.10}$	4	11
1035-276	19.0	2.168	0.8242	0.52 ± 0.02	1.08 ± 0.02	0.87 ± 0.02	<0.6	26	$18.81^{+0.15}_{-0.24}$	1	06
1037+0028	18.4	1.733	1.4244	1.767 ± 0.081	2.563 ± 0.031	2.171 ± 0.031	0.303 ± 0.042	4	$20.04^{+0.10}_{-0.14}$	4	11
1038+064	16.7	1.265	0.4416	<0.2	0.66 ± 0.05	0.57 ± 0.04	<0.2	2	$18.30^{+0.18}_{-0.30}$	1	AR
1040+123	17.3	1.028	0.6591	<0.2	0.58 ± 0.10	0.42 ± 0.10	<0.2	14	$18.38^{+0.05}_{-0.08}$	1	AR
1047-0047	18.4	0.740	0.5727	0.765 ± 0.130	1.063 ± 0.117	0.697 ± 0.094	0.055 ± 0.096	4	$19.36^{+0.17}_{-0.19}$	4	11
1048+0032	18.6	1.649	0.7203	1.252 ± 0.077	1.878 ± 0.063	1.636 ± 0.070	0.417 ± 0.085	4	$18.78^{+0.18}_{-0.48}$	4	11

TABLE 1 — *Continued*

QSO	m_V	z_{em}	z_{abs} MgII	$W_0^{\lambda 2600}$ (Å) FeII	$W_0^{\lambda 2796}$ (Å) MgII	$W_0^{\lambda 2803}$ (Å) MgII	$W_0^{\lambda 2852}$ (Å) MgI	Refs	$\log N(\text{HI})^b$	Sel ^c Crit	UV sp ^d source
1049+616	16.5	0.421	0.2255	<0.4	0.51 ± 0.03	0.56 ± 0.03	<0.1	18	< 18.00	1	06
...	0.3937	<0.1	0.34 ± 0.03	0.29 ± 0.03	...	18	< 18.00	1	06
1054-0020	18.3	1.021	0.8301	0.860 ± 0.049	1.156 ± 0.041	1.102 ± 0.041	0.333 ± 0.048	4	$18.95^{+0.09}_{-0.26}$	4	11
...	0.9514	0.408 ± 0.047	0.834 ± 0.047	0.506 ± 0.049	0.263 ± 0.053	4	$19.28^{+0.02}_{-0.02}$	1	11
1100-264	16.0	2.148	1.1872	0.04 ± 0.01	0.51 ± 0.01	0.28 ± 0.01	<0.2	13,27	$18.51^{+0.04}_{-0.03}$	1	AR
...	1.2028	<0.2	0.54 ± 0.02	0.43 ± 0.02	0.27 ± 0.05	13,27,28	$18.40^{+0.05}_{-0.04}$	1	AR
1107+0003	18.6	1.740	0.9545	0.868 ± 0.048	1.356 ± 0.066	1.187 ± 0.059	-0.044 ± 0.036	4	$20.26^{+0.09}_{-0.14}$	4	11
1107+0048	17.5	1.392	0.7404	2.375 ± 0.020	2.952 ± 0.025	2.809 ± 0.025	0.913 ± 0.032	4	$21.00^{+0.05}_{-0.05}$	4	11
...	1.0703	0.035 ± 0.038	0.532 ± 0.033	0.260 ± 0.031	0.026 ± 0.032	4	$18.60^{+0.03}_{-0.03}$	1	11
1109+0051	18.7	0.957	0.4181	...	1.361 ± 0.105	1.083 ± 0.110	0.198 ± 0.110	4	$19.08^{+0.22}_{-0.38}$	1	11
...	0.5520	0.934 ± 0.092	1.417 ± 0.085	1.193 ± 0.075	0.482 ± 0.094	4	$19.60^{+0.10}_{-0.12}$	4	11
1110+0048	18.6	0.761	0.5604	2.132 ± 0.117	2.273 ± 0.089	2.623 ± 0.083	0.436 ± 0.083	4	$20.20^{+0.18}_{-0.09}$	4	11
1112+0013	18.8	1.433	1.2420	0.667 ± 0.106	2.158 ± 0.083	1.752 ± 0.079	0.029 ± 0.054	4	$19.30^{+0.02}_{-0.15}$	4	11
1115+080	17.0	1.732	1.0431	<0.1	0.31 ± 0.03	0.18 ± 0.03	<0.2	2	$18.62^{+0.02}_{-0.02}$	1	AR
1127-145	16.9	1.187	0.3130	1.14 ± 0.27	2.21 ± 0.12	1.90 ± 0.12	1.14 ± 0.12	29	$21.71^{+0.07}_{-0.08}$	1	06
1137+660	16.3	0.652	0.1164	<0.2	0.50 ± 0.14	0.53 ± 0.12	<0.2	30	$18.60^{+0.10}_{-0.12}$	1	AR
1148+386	17.0	1.304	0.5533	<0.2	0.92 ± 0.05	0.99 ± 0.05	<0.2	2	< 18.00	1	06
1206+459	15.5	1.155	0.9276	0.08 ± 0.02	0.88 ± 0.02	0.79 ± 0.04	0.04 ± 0.02	2,7	$19.04^{+0.04}_{-0.04}$	1	AR
1209+107	17.8	2.193	0.3930	<0.4	1.00 ± 0.07	0.54 ± 0.09	<0.2	31	$19.46^{+0.08}_{-0.08}$	1	AR
...	0.6295	1.50 ± 0.20	2.92 ± 0.23	2.05 ± 0.18	<0.4	31	$20.30^{+0.18}_{-0.30}$	1	AR
1213-002	17.0	2.691	1.5543	1.11 ± 0.09	2.09 ± 0.06	1.65 ± 0.06	<0.2	2	$19.56^{+0.05}_{-0.02}$	1	06
1220-0040	18.5	1.411	0.9746	1.005 ± 0.098	1.952 ± 0.145	1.793 ± 0.125	0.143 ± 0.101	4	$20.20^{+0.05}_{-0.09}$	4	11
1222+228	16.6	2.048	0.6681	<0.1	0.43 ± 0.04	0.41 ± 0.04	<0.1	6	$18.59^{+0.03}_{-0.03}$	1	06
1224+0037	18.7	1.482	1.2346	0.950 ± 0.091	1.093 ± 0.072	1.028 ± 0.069	0.119 ± 0.063	4	$20.88^{+0.04}_{-0.06}$	4	11
...	1.2665	1.634 ± 0.183	2.094 ± 0.062	1.985 ± 0.073	0.330 ± 0.077	4	$20.00^{+0.08}_{-0.05}$	4	11
1225+0035	18.9	1.226	0.7730	1.316 ± 0.141	1.744 ± 0.138	1.447 ± 0.150	0.929 ± 0.135	4	$21.38^{+0.11}_{-0.12}$	4	11
1226+105	18.5	2.305	0.9376	0.86	1.36	1.20	...	3	$19.41^{+0.12}_{-0.18}$	3	09
1229-021	16.8	1.038	0.7571	...	0.52 ± 0.07	0.48 ± 0.07	<0.1	14	$18.36^{+0.09}_{-0.08}$	1	AR
1241+176	15.9	1.282	0.5505	0.24 ± 0.05	0.48 ± 0.02	0.37 ± 0.05	0.10 ± 0.03	2,7	$18.90^{+0.07}_{-0.09}$	1	AR
1246-057	16.7	2.224	1.2015	0.40 ± 0.03	0.90 ± 0.04	0.75 ± 0.04	<0.4	2	$18.91^{+0.03}_{-0.03}$	1	AR
...	1.6453	0.38 ± 0.06	0.52 ± 0.04	0.58 ± 0.04	<0.3	2	$18.89^{+0.02}_{-0.02}$	1	AR
1247+267	15.6	2.043	1.2232	...	0.48 ± 0.03	0.38 ± 0.02	0.11 ± 0.02	2	$19.87^{+0.01}_{-0.01}$	1	AR
1248+401	16.1	1.032	0.7730	0.25 ± 0.02	0.69 ± 0.01	0.50 ± 0.08	0.07 ± 0.02	2,7	$18.60^{+0.02}_{-0.02}$	1	AR
1254+047	16.4	1.018	0.5193	0.40 ± 0.05	0.46 ± 0.04	0.38 ± 0.04	<0.2	2	$18.86^{+0.06}_{-0.06}$	1	AR
1317+277	16.0	1.014	0.2887	...	0.33 ± 0.04	0.31 ± 0.04	<0.2	2	< 18.30	1	AR
...	0.6601	0.13 ± 0.02	0.34 ± 0.01	0.33 ± 0.04	0.03 ± 0.01	2,7	$18.57^{+0.02}_{-0.02}$	1	AR
1323-0021	18.2	1.390	0.7160	1.452 ± 0.077	2.229 ± 0.071	1.864 ± 0.066	0.940 ± 0.069	4	$20.54^{+0.15}_{-0.15}$	4	11
1323+655	17.5	1.624	1.5181	...	0.57	0.53	<0.1	3	$18.56^{+0.02}_{-0.02}$	1	06
...	1.6101	0.88	2.20	1.85	0.16	3	high <i>b</i>	1	06
1327-206	17.0	1.165	0.8526	0.76 ± 0.27	2.11	1.48	<0.2	32,33	$19.40^{+0.02}_{-0.02}$	1	AR
1329+412	17.2	1.937	1.2820	...	0.49 ± 0.05	0.31 ± 0.05	<0.3	2	$19.46^{+0.09}_{-0.10}$	1	06
...	1.6011	<0.2	0.70 ± 0.04	0.35 ± 0.04	<0.2	2	$19.04^{+0.04}_{-0.04}$	1	06
1338+416	16.1	1.204	0.6213	<0.1	0.31 ± 0.05	0.17 ± 0.04	<0.3	2	$19.08^{+0.03}_{-0.04}$	1	AR
1341+0059	18.8	1.714	1.1176	0.929 ± 0.119	1.711 ± 0.154	1.145 ± 0.133	0.414 ± 0.088	4	$19.93^{+0.11}_{-0.08}$	4	11

TABLE 1 — *Continued*

QSO	m_V	z_{em}	z_{abs} MgII	$W_0^{\lambda 2600}$ (Å) FeII	$W_0^{\lambda 2796}$ (Å) MgII	$W_0^{\lambda 2803}$ (Å) MgII	$W_0^{\lambda 2852}$ (Å) MgI	Refs	$\log N(\text{HI})^b$	Sel ^c Crit	UV sp ^d source
1342–0035	18.2	0.787	0.5380	1.453 ± 0.090	2.256 ± 0.068	1.882 ± 0.083	0.780 ± 0.088	4	$19.78^{+0.12}_{-0.14}$	4	11
1345–0023	17.6	1.095	0.6057	0.635 ± 0.049	1.177 ± 0.049	1.219 ± 0.052	0.155 ± 0.043	4	$18.85^{+0.15}_{-0.24}$	4	11
1354+195	16.0	0.719	0.4566	0.32 ± 0.04	0.89 ± 0.04	0.82 ± 0.04	0.16 ± 0.03	2	$18.54^{+0.04}_{-0.04}$	1	AR
1354+258	18.0	2.006	0.8585	<0.2	1.00	0.86	<0.1	3	$18.57^{+0.07}_{-0.08}$	1	06
...	0.8856	<0.2	0.81	0.57	<0.2	3	$18.76^{+0.10}_{-0.13}$	1	06
...	1.4205	0.55	0.61	0.50	0.20	3	$21.51^{+0.03}_{-0.03}$	1	06
1419–0036	18.3	0.969	0.6238	0.075 ± 0.083	0.597 ± 0.069	0.476 ± 0.071	0.106 ± 0.073	4	$19.04^{+0.07}_{-0.14}$	1	11
...	0.8206	0.848 ± 0.073	1.145 ± 0.057	0.963 ± 0.064	0.167 ± 0.067	4	$18.78^{+0.26}_{-0.23}$	4	11
1420–0054	18.9	1.458	1.3475	1.079 ± 0.097	1.532 ± 0.108	1.227 ± 0.104	0.365 ± 0.105	4	$20.90^{+0.05}_{-0.06}$	4	11
1421+330	16.7	1.906	0.9026	...	1.08 ± 0.03	0.85 ± 0.03	...	2	$18.85^{+0.01}_{-0.01}$	2	09
...	1.1725	<0.1	0.54 ± 0.03	0.40 ± 0.03	<0.1	2	$18.79^{+0.01}_{-0.01}$	1	09
1426+0051	18.8	1.333	0.7352	0.275 ± 0.072	0.857 ± 0.080	0.751 ± 0.085	0.047 ± 0.086	4	$18.85^{+0.03}_{-0.03}$	1	11
...	0.8424	1.081 ± 0.109	2.618 ± 0.125	1.972 ± 0.109	0.454 ± 0.131	4	$19.65^{+0.09}_{-0.07}$	4	11
1431–0050	18.1	1.190	0.6085	1.239 ± 0.074	1.886 ± 0.076	1.581 ± 0.079	0.203 ± 0.060	4	$19.18^{+0.30}_{-0.27}$	4	11
...	0.6868	0.123 ± 0.059	0.613 ± 0.066	0.283 ± 0.057	0.049 ± 0.059	4	$18.40^{+0.06}_{-0.08}$	1	11
1436–0051	18.5	1.275	0.7377	1.051 ± 0.095	1.142 ± 0.084	1.146 ± 0.089	0.625 ± 0.081	4	$20.08^{+0.10}_{-0.12}$	4	11
...	0.9281	0.662 ± 0.080	1.174 ± 0.065	0.971 ± 0.063	0.132 ± 0.072	4	< 18.82	4	11
1437+624	19.0	1.090	0.8723	...	0.71 ± 0.09	0.64 ± 0.09	...	14	< 18.00	2	09
1455–0045	18.0	1.378	1.0929	1.273 ± 0.043	1.625 ± 0.056	1.577 ± 0.061	0.373 ± 0.055	4	$20.08^{+0.03}_{-0.08}$	4	11
1501+0019	18.1	1.930	1.4832	1.481 ± 0.042	2.168 ± 0.052	1.853 ± 0.052	0.952 ± 0.054	4	$20.85^{+0.11}_{-0.15}$	4	11
1517+239	16.4	1.903	0.7382	<0.1	0.30 ± 0.04	0.34 ± 0.06	...	6	$18.72^{+0.03}_{-0.03}$	1	AR
1521–0009	19.0	1.318	0.9590	1.610 ± 0.090	1.848 ± 0.096	1.588 ± 0.093	0.944 ± 0.107	4	$19.40^{+0.08}_{-0.14}$	4	11
1525+0026	17.0	0.801	0.5674	1.140 ± 0.053	1.852 ± 0.035	1.525 ± 0.035	0.359 ± 0.042	4	$19.78^{+0.07}_{-0.08}$	4	11
1537+0021	19.1	1.754	1.1782	2.087 ± 0.113	2.502 ± 0.102	2.732 ± 0.104	0.517 ± 0.115	4	$20.18^{+0.08}_{-0.10}$	4	11
...	1.6455	1.498 ± 0.074	2.272 ± 0.111	2.172 ± 0.087	0.553 ± 0.079	4	$20.48^{+0.22}_{-0.18}$	4	11
1554–203	19.2	1.947	0.7869	...	0.73	0.76	...	3	< 19.00	2	09
1622+239	17.5	0.927	0.6561	1.02 ± 0.05	1.45 ± 0.03	<1.7	0.29 ± 0.03	2,7	$20.36^{+0.07}_{-0.08}$	1	AR
...	0.8913	1.02 ± 0.15	1.55 ± 0.08	1.27 ± 0.08	0.31 ± 0.03	2	$19.23^{+0.02}_{-0.03}$	1	AR
1623+269	16.0	2.521	0.8881	0.21 ± 0.02	0.93 ± 0.03	0.75 ± 0.04	0.14 ± 0.02	6	$18.66^{+0.02}_{-0.03}$	1	06
1629+120	18.4	1.792	0.5313	0.71 ± 0.10	1.40 ± 0.07	1.35 ± 0.07	0.31 ± 0.08	14	$20.70^{+0.08}_{-0.10}$	3	09
...	0.9004	0.63 ± 0.10	1.20 ± 0.09	0.69 ± 0.09	...	3,14	$19.70^{+0.03}_{-0.04}$	3	09
1634+706	14.9	1.335	0.9902	0.13 ± 0.01	0.56 ± 0.01	0.42 ± 0.03	0.06 ± 0.01	2,7	$18.34^{+0.02}_{-0.02}$	1	AR
1704+608	15.3	0.371	0.2220	...	0.55 ± 0.03	0.33 ± 0.03	<0.2	18	$18.23^{+0.05}_{-0.05}$	1	AR
1712+5559	18.7	1.358	1.1584	0.605 ± 0.053	0.889 ± 0.058	0.847 ± 0.061	0.227 ± 0.063	4	$19.54^{+0.06}_{-0.15}$	1	11
...	1.2093	1.173 ± 0.054	1.742 ± 0.058	1.388 ± 0.058	...	4	$20.72^{+0.05}_{-0.05}$	4	11
1714+5757	18.6	1.252	0.7481	0.880 ± 0.108	1.099 ± 0.084	0.864 ± 0.085	0.071 ± 0.099	4	$19.23^{+0.17}_{-0.33}$	4	11
1715+5747	18.3	0.697	0.5579	0.532 ± 0.095	1.001 ± 0.067	0.813 ± 0.075	0.295 ± 0.073	4	$19.18^{+0.15}_{-0.18}$	4	11
1716+5654	19.0	0.937	0.5301	1.404 ± 0.161	1.822 ± 0.130	1.329 ± 0.108	0.081 ± 0.122	4	$19.98^{+0.20}_{-0.28}$	4	11
1722+5442	18.8	1.215	0.6338	0.588 ± 0.096	1.535 ± 0.098	1.350 ± 0.093	0.203 ± 0.099	4	$19.00^{+0.30}_{-0.22}$	4	11
1727+5302	18.3	1.444	0.9448	2.188 ± 0.116	2.832 ± 0.070	2.511 ± 0.071	0.988 ± 0.067	4	$21.16^{+0.04}_{-0.05}$	4	11
...	1.0312	0.755 ± 0.114	0.922 ± 0.057	1.181 ± 0.079	0.331 ± 0.095	4	$21.41^{+0.03}_{-0.03}$	4	11
1729+5758	17.5	1.342	0.5541	1.015 ± 0.058	1.836 ± 0.046	1.608 ± 0.046	0.121 ± 0.044	4	$18.60^{+0.18}_{-0.43}$	4	11
1733+5533	18.0	1.072	0.9981	1.344 ± 0.056	2.173 ± 0.069	2.004 ± 0.071	0.362 ± 0.080	4	$20.70^{+0.04}_{-0.03}$	4	11
1736+5938	18.8	1.410	1.0664	1.439 ± 0.092	2.177 ± 0.104	2.039 ± 0.110	...	4	$20.00^{+0.08}_{-0.10}$	4	11

TABLE 1 — *Continued*

QSO	m_V	z_{em}	z_{abs} MgII	$W_0^{\lambda 2600}$ (Å) FeII	$W_0^{\lambda 2796}$ (Å) MgII	$W_0^{\lambda 2803}$ (Å) MgII	$W_0^{\lambda 2852}$ (Å) MgI	Refs	$\log N(\text{HI})^b$	Sel ^c Crit	UV sp ^d source
1821+107	17.3	1.364	1.2528	<0.3	0.71 ± 0.04	0.48 ± 0.03	0.09 ± 0.02	2	high <i>b</i>	1	06
1857+566	17.3	1.578	0.7151	...	0.65	0.64	...	3	$18.56^{+0.05}_{-0.06}$	2	09
...	1.2345	0.55	0.82	0.70	...	3	$18.46^{+0.04}_{-0.06}$	3	09
1901+319	17.5	0.635	0.3901	00.0	0.45 ± 0.04	0.15 ± 0.04	<0.1	14	< 18.00	1	06
2003-025	19.0	1.457	1.2116	1.27 ± 0.14	2.65 ± 0.14	2.17 ± 0.14	...	14	$19.32^{+0.06}_{-0.07}$	3	09
...	1.4106	0.34 ± 0.08	0.74 ± 0.07	0.62 ± 0.07	...	14	$20.54^{+0.15}_{-0.24}$	2	09
2048+196	18.5	2.367	1.1157	1.31	1.52	1.28	...	3	$19.26^{+0.05}_{-0.08}$	3	09
2128-123	16.1	0.501	0.4297	0.27 ± 0.05	0.41 ± 0.01	0.37 ± 0.05	0.16 ± 0.03	13,7	$19.18^{+0.03}_{-0.03}$	1	AR
2145+067	16.5	0.999	0.7908	0.04 ± 0.01	0.48 ± 0.02	0.41 ± 0.06	<0.04	2,7	$18.43^{+0.03}_{-0.03}$	1	AR
2149+212	19.0	1.538	0.9114	0.95	0.72	0.62	...	3	$20.70^{+0.08}_{-0.10}$	3	09
...	1.0023	1.00	2.46	1.70	...	3	$19.30^{+0.02}_{-0.05}$	3	09
2212-299	17.4	2.706	0.6329	...	1.26	1.00	...	3	$19.75^{+0.03}_{-0.03}$	2	09
2223-052	18.4	1.404	0.8472	<0.4	0.65	0.42	<0.2	34,35	$18.48^{+0.41}_{-0.88}$	1	AR
2326-477	16.8	1.306	1.2608	<0.1	0.50 ± 0.04	0.38 ± 0.04	<0.1	13	$18.36^{+0.41}_{-0.76}$	1	AR
2328+0022	17.9	1.308	0.6519	1.258 ± 0.065	1.896 ± 0.077	1.484 ± 0.073	0.550 ± 0.079	4	$20.32^{+0.06}_{-0.07}$	4	11
2331+0038	17.8	1.486	1.1414	1.437 ± 0.064	3.007 ± 0.071	2.417 ± 0.066	0.579 ± 0.060	4	$20.00^{+0.04}_{-0.05}$	4	11
2334+0052	18.2	1.040	0.4713	1.113 ± 0.128	1.226 ± 0.107	1.281 ± 0.091	0.301 ± 0.089	4	$20.65^{+0.12}_{-0.18}$	4	11
2339-0029	18.6	1.340	0.9664	1.715 ± 0.072	2.932 ± 0.074	2.530 ± 0.076	0.882 ± 0.090	4	$20.48^{+0.07}_{-0.10}$	4	11
2352-0028	18.2	1.628	0.8730	0.122 ± 0.080	1.254 ± 0.095	0.816 ± 0.075	-0.048 ± 0.091	4	$19.18^{+0.08}_{-0.10}$	1	11
...	1.0318	1.494 ± 0.074	2.160 ± 0.102	1.714 ± 0.110	0.128 ± 0.119	4	$19.81^{+0.14}_{-0.11}$	4	11
...	1.2467	0.896 ± 0.132	2.926 ± 0.088	2.261 ± 0.120	0.087 ± 0.067	4	$19.60^{+0.18}_{-0.30}$	4	11
2353-0028	17.9	0.765	0.6044	1.024 ± 0.104	1.601 ± 0.082	1.292 ± 0.083	0.606 ± 0.080	4	$21.54^{+0.15}_{-0.15}$	4	11

REFERENCES. — (1) Lanzetta, Turnshek, & Wolfe 87. (2) SS92. (3) Barthel, Tytler, & Thomson 1990. (4) Nestor 2004. (5) Steidel 1990. (6) Sargent, Boksenberg, & Steidel 1988. (7) Churchill et al. 2000. (8) Sargent, Young, & Boksenberg 1982. (9) Sargent, Steidel, & Boksenberg 1989. (10) Bergeron & D'Odorico 1986. (11) Womble et al. 1990. (12) Wright et al. 1982. (13) Pettijean & Bergeron 1990. (14) Aldcroft, Bechtold, & Elvis 1994. (15) Tytler et al. 1987. (16) Boksenberg, Carswell, & Sargent 1979. (17) Khare et al. 2004. (18) Boissé et al. 1992. (19) Falomo 1990. (20) Wills 1978. (21) Ulrich & Owen 1977. (22) Foltz et al. 1986. (23) Bergeron & Boissé 1984. (24) Caulet 1989. (25) Wills & Wills 1980. (26) Dinshaw & Impey 1996. (27) Jannuzzi et al. 1998. (28) Boissé & Bergeron, 1985. (29) Bergeron & Boissé 1991. (30) Bahcall et al. 1993. (31) Young, Sargent, & Boksenberg 1982. (32) Kunth & Bergeron 1984. (33) Bergeron, D'Odorico, & Kunth 1987. (34) Le Brun et al. 1993. (35) Miller & French 1978.

^a For systems other than those from Nestor (2004), upper limits are either given by the authors or estimated by us from the published spectrum. If the line is part of a blend, then the rest equivalent width entered is an upper limit. The upper limit is a 1σ upper limit if estimated by us from the published spectrum. In some cases, the absorption line ($\lambda 2600$ or $\lambda 2852$) was clearly visible in the spectrum but was not identified by the authors since the rest equivalent width of the line did not meet their detection criterion, usually 5σ . In these cases, we estimated the equivalent width of the line from the spectrum and tabulated the measurement as an upper limit. The trends that we have established are evident from the measurements of rest equivalent widths by the authors of the published spectra; our upper limit measurements only serve to provide a certain degree of completeness to our sample and, in fact, do not indicate or contribute to any trends by themselves. We note that the quasar 0151+045 was erroneously included in Table 4 of RT00. The MgII system towards this quasar was detected after the galaxy-quasar pair was known and is, therefore, a biased system. In addition, the $z_{\text{abs}} = 0.213$ system towards 1148+386 and the $z_{\text{abs}} = 0.1634$ system towards 1704+608 were flagged as doubtful systems by Boissé et al. (1992). Finally, the nature of the $z_{\text{abs}} = 1.3284$ system towards 1331+170 was deemed inconclusive from the low signal-to-noise ratio IUE spectrum. Therefore, these four were eliminated from our current MgII sample.

^b In two cases (the $z_{\text{abs}} = 1.6101$ system towards 1329+412 and the $z_{\text{abs}} = 1.2528$ system towards 1821+107), the HI column density could not be determined because the Ly α and higher order Lyman lines could not be fit with a unique value of $N(\text{HI})$ under the assumption that the lines are damped. A large *b* value (greater than 100 km s^{-1}) was necessary in both cases. Thus, it is clear that these systems are not DLAs. These are flagged as “high *b*” systems.

^c Flag for $W_0^{\lambda 2796}$ selection criterion used in the determination of n_{DLA} . See §4.

^d Source for UV spectrum from which Ly α information was obtained. AR: HST or IUE archive, 06: *HST*-cycle 6 program 6577, P.I. Rao, 09: *HST*-cycle 9 program 8569, P.I. Rao, 11: *HST*-cycle 11 program 9382, P.I. Rao